A Twining Company

2800 Wilderness Place Suite A
Boulder, CO 80301
T: 303.938.0166
www.drpcinc.com

Petrographic Investigation of Concrete Cores Extracted from Aprons at the Billings Logan International Airport Located in Billings, Montana

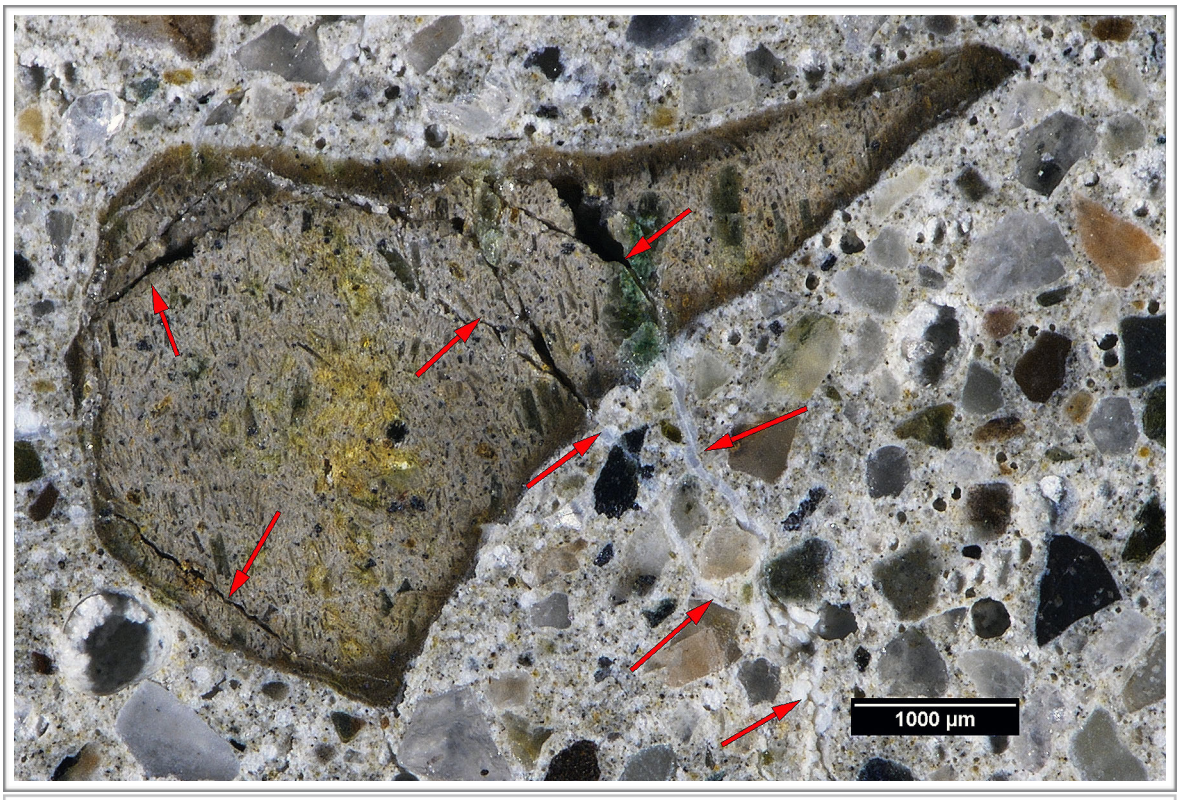

Prepared for

Michael Berry, Ph.D.
Montana State University
Bozeman, Montana

Prepared by

Chunyu Qiao, Ph.D.
David Rothstein, Ph.D., P.G., FACI
Report No. 197382.d
23 December 2019

EXECUTIVE SUMMARY

Two (2) concrete cores extracted from the Billings Logan International Airport located in Billings, Montana are subjects of petrographic examination per ASTM C856. The purpose of the investigation is to characterize the severity of ASR in the concrete represented by the cores and to determine the cause(s) of cracking observed in the concrete.

The findings from this scope of work indicate the following three cracking mechanisms:

- Early age cracks that are up to 750 µm (30 mil) wide which cut sub-vertically up to 25 m (1 in.) from the top surface. These cracks mainly cut around aggregate particles and are mostly free of secondary deposits but occasionally show evidence of carbonation along their walls. These cracks are typical of early age drying shrinkage. They are significant from a durability perspective because they facilitate the ingress of moisture which is associated with both freeze-thaw damage and alkali-silica reaction (ASR).
- Sub-horizontal cracks that range up to 1 mm (40 mil) wide cut across the full width of both cores. These cracks mainly cut around aggregate particles and show occasional splays and bifurcations. Deposits of ettringite were observed in voids along the walls of the cracks. These characteristics are typical of cracking due to freeze-thaw damage. Sample 2 shows more severe freeze-thaw damage compared to Sample 5. While the deposits of ettringite are not associated with an internal expansion mechanism associated with the observed cracking, they indicate high levels of moisture along the walls of the cracks. Filling of voids with ettringite may also increase the susceptibility of the concrete to freeze-thaw damage. Segments of these cracks occasionally cut through aggregate particles and contain minor deposits of ASR gel.
- Cracking and microcracking from alkali-silica reaction (ASR) was observed commonly in both cores. These cracks range up to 50-55 mm (2 - 2 ¼ in.) long and 200 µm (8 mil) wide. These cracks and microcracks are filled with ASR gel and radiate outward from or cut through reactive aggregate particles. The cracks and microcracks are interconnected and form complex networks of cracks and microcracks. Cracks due to ASR are more narrow than the sub-horizontal cracks due to freeze-thaw damage. They commonly cut into cracks associated with freeze-thaw damage, indicating that at least some ASR damage occurred after the presence of freeze-thaw damage. Some examples of mutually cross-cutting relationships between cracks associated with ASR and freeze-thaw damage indicate that both mechanisms also operated coevally.

Both cores contain coarse aggregate that consists of a siliceous gravel. The reactive components present in the aggregate include rhyolite, quartzite, chert and andesite. Reactive particles are observed most commonly in the coarse and occasionally in the fine aggregate. The ASR is at Stage V using a qualitative scale described by Katayama et al. [**1**] and is severe using a qualitative scale described by DRP.

Table ES1. DRP criteria for severity of ASR damage-1

Severity	Criteria
Absent	No reaction rims, microcracks or cracks associated with ASR
Negligible	Only reaction rims observed
Trace	ASR gel rarely observed lining voids near aggregate particles
Minor	ASR gel in voids near reactive particles or rimming reactive particles; microcracks with ASR gel rarely to occasionally observed
Moderate	Microcracks filled with ASR gel commonly observed
Severe	Cracks (> 100 µm wide) due to ASR observed

Table ES2. Petrographic stages of ASR (after [1])-1

Stage	Criteria
I	Formation of reaction rims within aggregate particles.
II	Exudation of ASR sol/gel around aggregate particles. Darkening of paste around aggregate particles.
III	Cracking of aggregate; ASR gel may line or fill crack.
IV	Propagation of cracks from reacted aggregate into paste. ASR gel may line or fill crack; crack width grows.
V	Filling/lining of ASR gel into distant air voids. Note crack width for advanced damage.

The cores represent concrete mixtures that are similar except for the composition of the paste and the nominal top size of the aggregate. In Sample 2 the paste contains hydrated portland cement with no fly ash, slag cement or other supplemental cementitious materials observed. In Sample 5 the paste contains portland cement and fly ash; no slag cement of other supplemental cementitious materials observed. The coarse aggregate is a crushed siliceous gravel with a 25 mm (1 in.) nominal top size in Sample 2 and a 19 mm (¾ in.) nominal top size in Sample 5. The coarse aggregate is siliceous in composition and consists primarily of rhyolite, granitic rocks, quartzite and chert with minor andesite and basalt. The fine aggregate is a natural sand that consists of rocks similar to those in the coarse aggregate. Both cores are air entrained with ~ 6% estimated total air content.

1 Katayama, T., Sarai, Y. and Sawaguchi, H., 2016, Diagnosis of ASR in Airport Pavements in Japan—Early-Expansive Sand Aggregate Missed by Conventional Testing, *Proceedings of the 15th International Conference on Alkali-Aggregate Reactions*, Sao Paolo, Brazil.

1.0 INTRODUCTION

Michael Berry, Ph.D., Associate Professor at the Department of Civil Engineering at Montana State University (**MSU**) located in Bozeman, Montana requested DRP, a Twining Company (**DRP**) to investigate the condition of concrete represented by cores extracted from two aprons at the Billings Logan International Airport. The purpose of the investigation is to characterize to determine the cause(s) of cracking observed in the concrete and to determine if there is evidence of alkali-silica reaction (ASR). Professor Berry indicated that there have been no documented cases of ASR damage in the state of Montana.

On 12 November 2019 **DRP** received four (4) cores from **MSU**. The cores were designated as Sample 2, Sample 3, Sample 5 and Sample 6 and assigned **DRP** sample numbers 23YD10291 - 23YD10294, respectively.

No information was provided regarding the age of the original construction, concrete mix designs used for the original construction, construction specifications or records of testing done during or after construction.

2.0 Scope of Work

The testing involved petrographic examinations on Sample 2 and Sample 5 according to ASTM C856 [**2**]. Air contents were estimated based on visual and microscopical observations but were not measured per ASTM C457 [**3**]. *Appendix A* and *Appendix B* contain the notes, photographs and micrographs from the petrographic examinations and *Appendix C* describes the procedures used to perform this scope of work. The petrographic work was performed by a senior petrographer and reviewed by the principal petrographer.

2 *Standard Practice for Petrographic Examination of Hardened Concrete.* Annual Book of ASTM Standards, Vol. 4.02., ASTM C856-18.

3 *Standard Test Method for Microscopical Determination of Parameters of the Air-Void System in Hardened Concrete*, Annual Book of ASTM Standards, Vol. 4.02, ASTM C457-16.

3.0 FINDINGS

3.1 ***Orientation, Dimensions & As-Received Condition*** The cores are vertical in orientation, measure ~ 95 mm (3 ¾ in.) in diameter and range from 160 - 205 mm (6 ¼ - 8 in.) in length. The cores are hard and compact. The top surface of each core shows significant wear such that the original texture is not apparent and the bottom surface of each core is a fracture such that the cores represent a partial thickness of the aprons. Both cores were received in two pieces with a sub-horizontal fracture in the middle of the cores. White deposits of ASR gel were observed on the fracture surface and the bottom surface of both cores. **Figure 1** shows photographs of the cores in their as-received condition and the polished surface from each core. **Figure 2** shows photomicrographs of the top surface of each core. **Figure 3** shows photomicrographs of the white deposits on the fracture and bottom surface of each core.

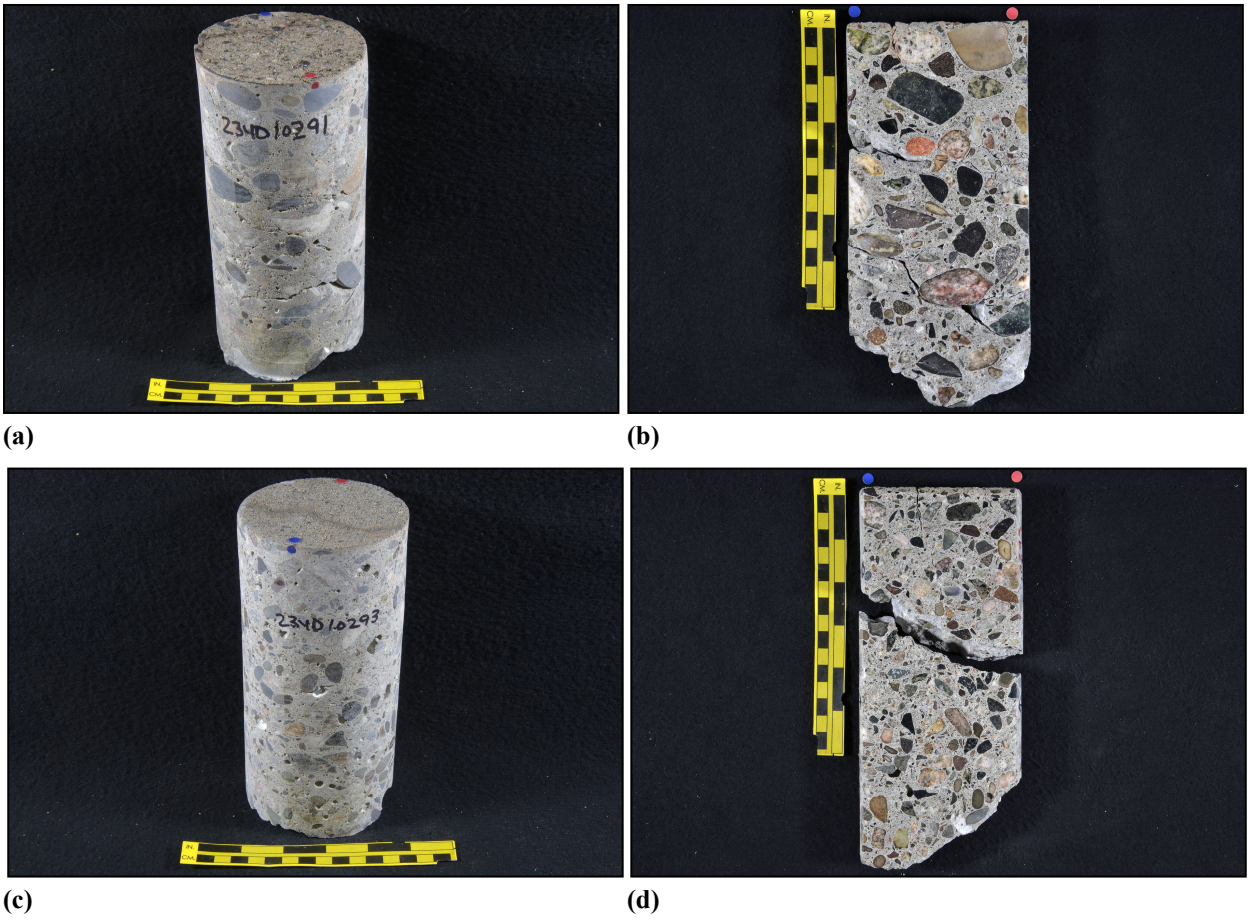

(a) **(b)**

(c) **(d)**

Figure 1. (a) Photograph showing oblique view of the top and side of Sample 2 in as-received condition. (b) Photograph showing the polished surface of Sample 2. (c) Photograph showing oblique view of the top and side of Sample 5 in as-received condition. (d) Photograph showing the polished surface of Sample 5. The red and blue dots indicate the orientation of the saw cuts used to prepare the sample for petrography. The small and large divisions on the yellow scale are in centimeters and inches, respectively.

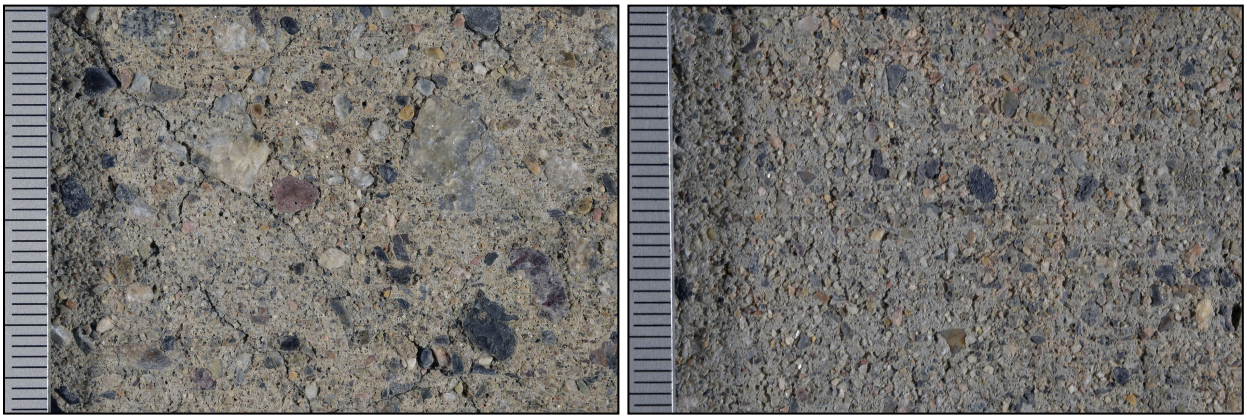

(a) (b)

Figure 2. Photograph showing the top surface of (a) Sample 2 and (b) Sample 5, respectively, in as-received condition. The scale in both images is in millimeters.

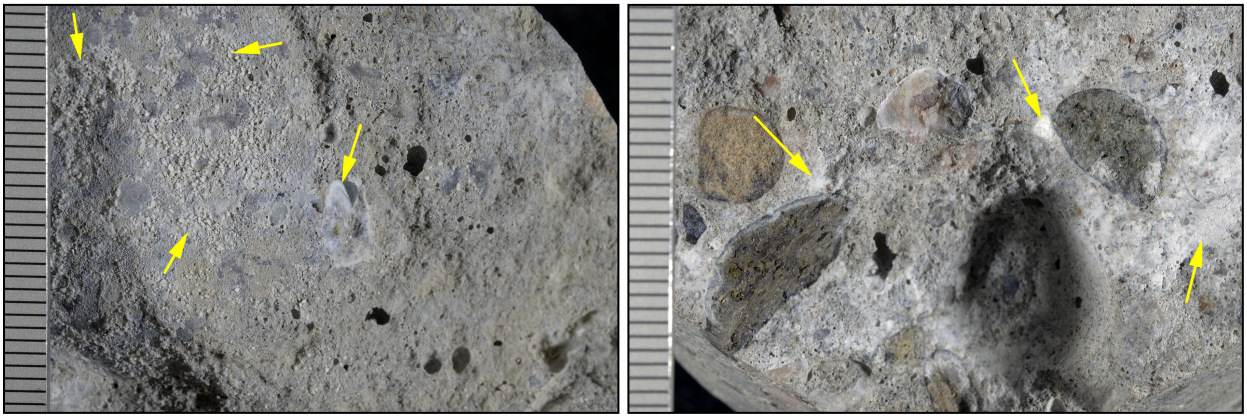

(a) (b)

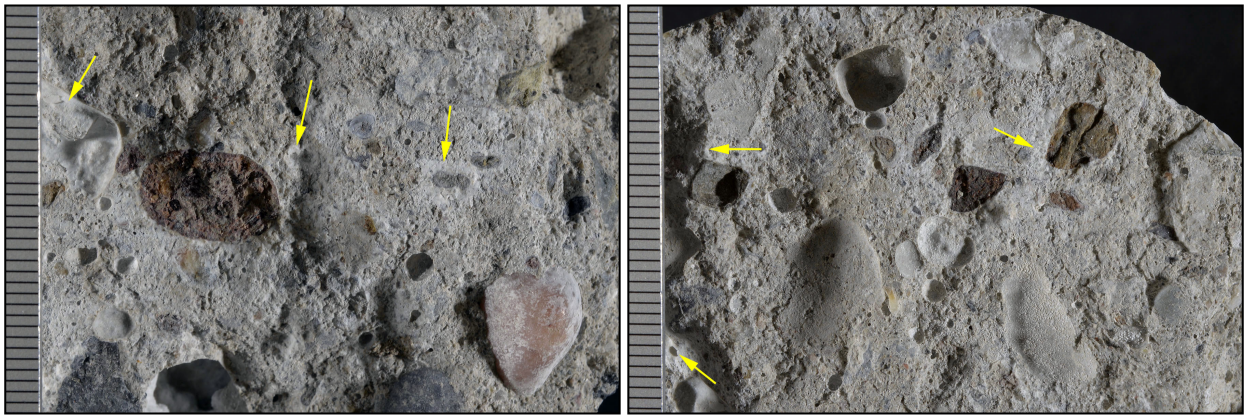

(c) (d)

Figure 3. Deposits of ASR gel (yellow arrows) on received surfaces. Photographs of Sample 2 showing ASR gel (a) on the fracture surface and (b) on the bottom surface of the core. Photographs of Sample 5 showing detail of ASR gel on the bottom surface of the core. The scale in each photograph is in millimeters.

3.2 ***Components: Paste*** The paste in Sample 2 contains hydrated portland cement with no fly ash or other supplemental cementitious materials, while the paste in Sample 5 contains hydrated portland cement with fly ash. The hydration is normal in both cores. The capillary porosity of the paste is moderate and relatively consistent. The water-cementitious materials ratio (w/cm) of the paste was not estimated because of evidence of significant alteration of the paste by mechanisms such as ASR and ettringite mineralization. Both of these mechanisms require the ingress of moisture, which obscures the original w/cm. **Figure 4** and **Figure 5** show photomicrographs of the paste in Sample 2 and Sample 5, respectively. **Figure 6** shows transmitted fluorescent light photomicrographs of thin sections that indicate the capillary porosity of the paste in each core.

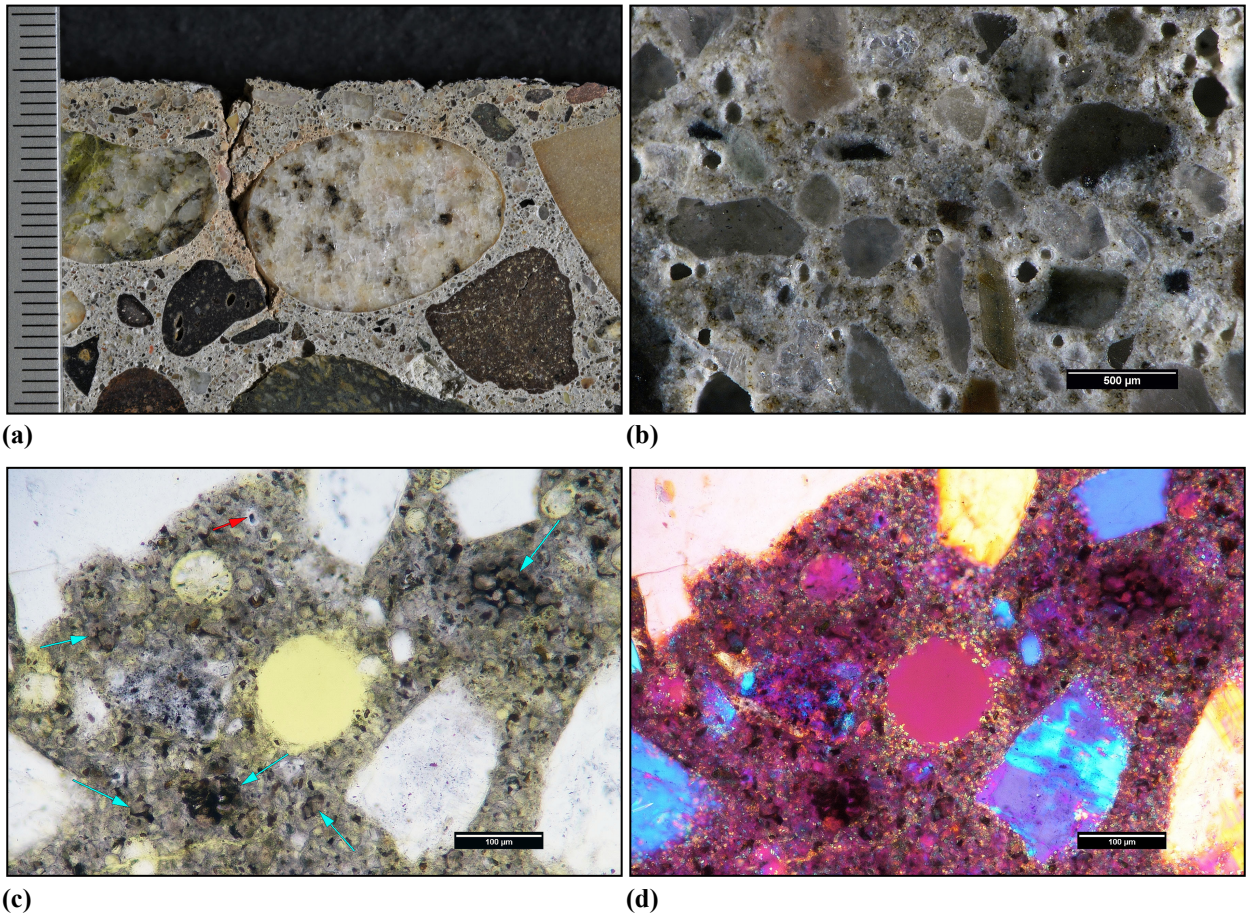

(a) (b)

(c) (d)

Figure 4. Paste characteristics in Sample 2. (a) Photograph of the polished surface showing overview of the paste near the top surface; scale in millimeters. (b) Reflected light photomicrograph of the polished surface showing the detail of paste in the middle of the core. (c) Plane-polarized transmitted light photomicrograph of thin section showing detail of the paste. The red and light blue arrows indicate alite and belite, respectively. (d) Cross-polarized transmitted light photomicrograph of thin section with gypsum plate inserted showing detail of the paste.

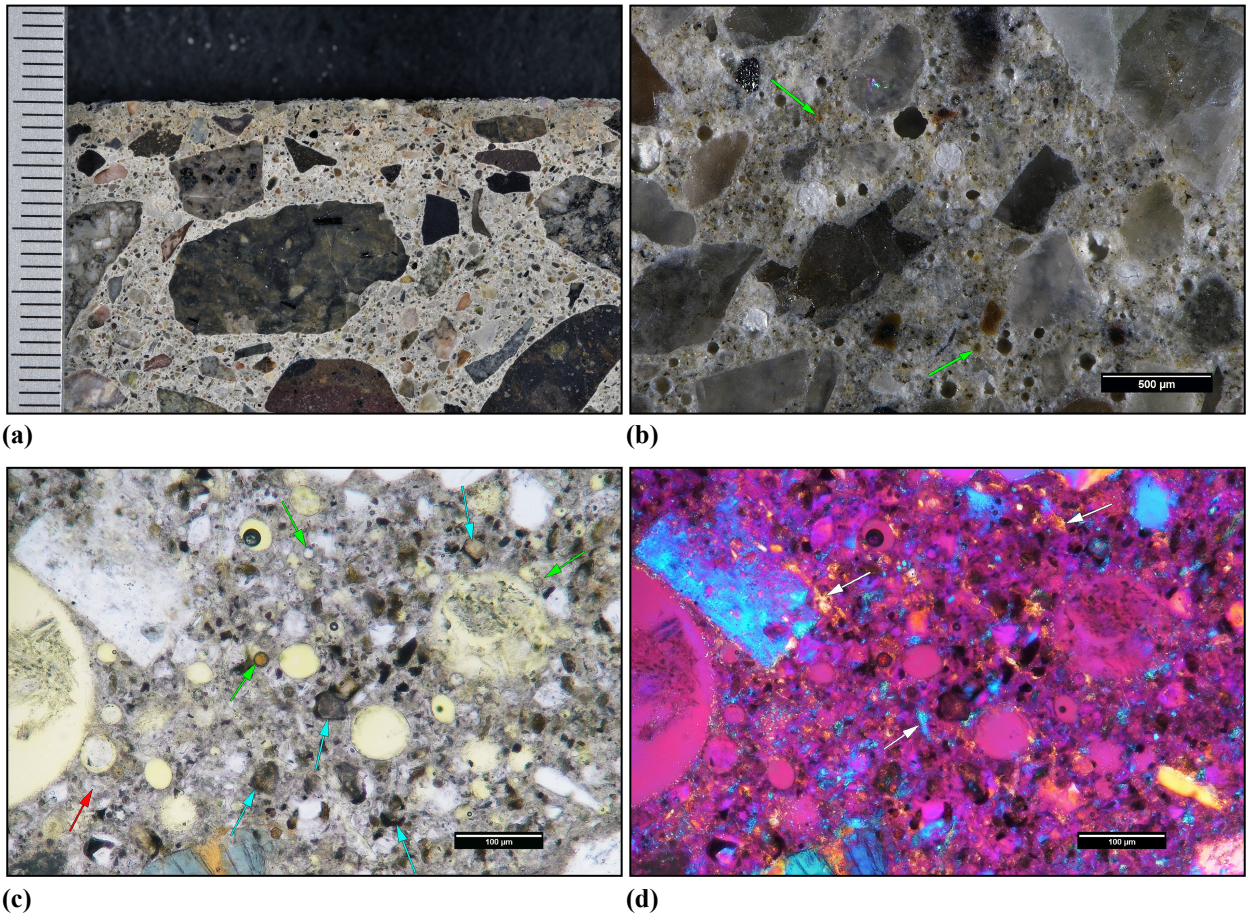

(a) (b)

(c) (d)

Figure 5. Paste characteristics in Sample 5. (a) Photograph of the polished surface showing overview of the paste near the top surface; scale in millimeters. (b) Reflected light photomicrograph of the polished surface showing the detail of paste in the middle of the core. The green arrows in (b) indicate fly ash. (c) Plane-polarized transmitted light photomicrograph of thin section showing detail of the paste. The red, light blue and green arrows indicate alite, belite and fly ash, respectively. (d) Cross-polarized transmitted light photomicrograph of thin section with gypsum plate inserted showing detail of the paste; the white arrows indicate calcium hydroxide.

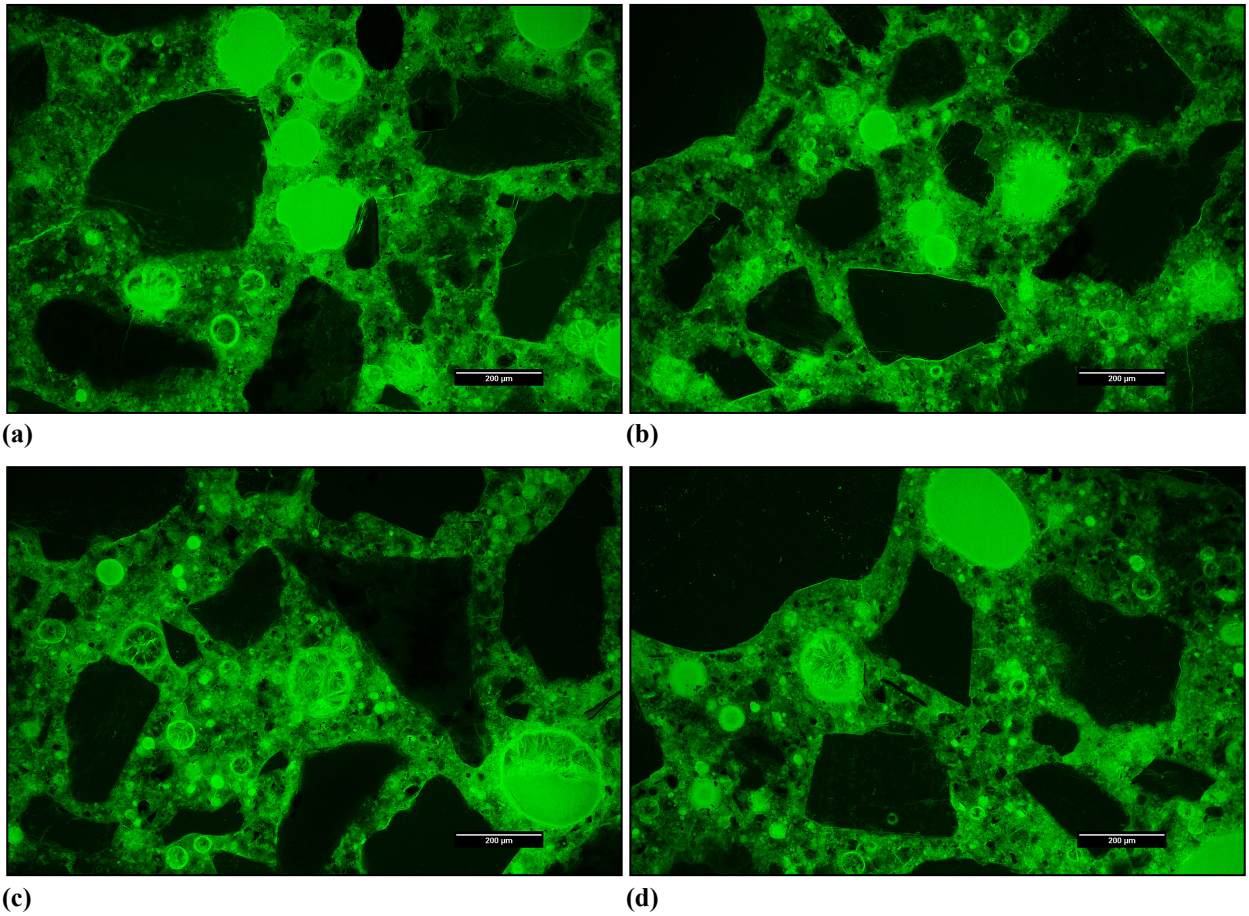

(a) (b)

(c) (d)

Figure 6. (a), (b) Transmitted fluorescent light photomicrographs of thin section from the Sample 2 showing detail of paste. (c), (d) Transmitted fluorescent light photomicrographs of thin section from Sample 5 showing detail of paste. The green tone of the images is a function of the infiltration of the fluorescent epoxy, such that it is proportional to the capillary porosity of the material. The black areas correspond to aggregate that has very low porosity or effectively zero porosity and the bright circular areas represent voids that are 100% porosity. The variations in green between aggregate particles reflect variations in the capillary porosity or micro-density of the paste. Note ettringite in voids in the images.

3.3 ***Components: Air Voids*** Both cores are air-entrained and contain ~ 6% total air. Note that these air contents are estimated from visual and microscopical observations and were not measured in accordance with ASTM C457. The concrete is well consolidated. As discussed below, voids in both cores commonly contain deposits of ettringite. Occasional voids contain deposits of ASR gel.

3.4 ***Components: Aggregates*** The coarse aggregate is a crushed gravel with a nominal top size of 25 mm (1 in.) in Sample 2 and 19 mm (1 in.) in Sample 5, respectively (**Figure 7**). The gradation and distribution are relatively even in both cores. The aggregate is siliceous in composition and consists primarily of rhyolite, granitic rocks, quartzite and chert with trace amounts of andesite and basalt. The fine aggregate is a natural sand that consists mostly of siliceous rocks similar to that observe in coarse aggregate. Both cores show evidence of severe ASR that involves rhyolite, chert, quartzite and andesite in coarse aggregate commonly but also occasionally in the fines.

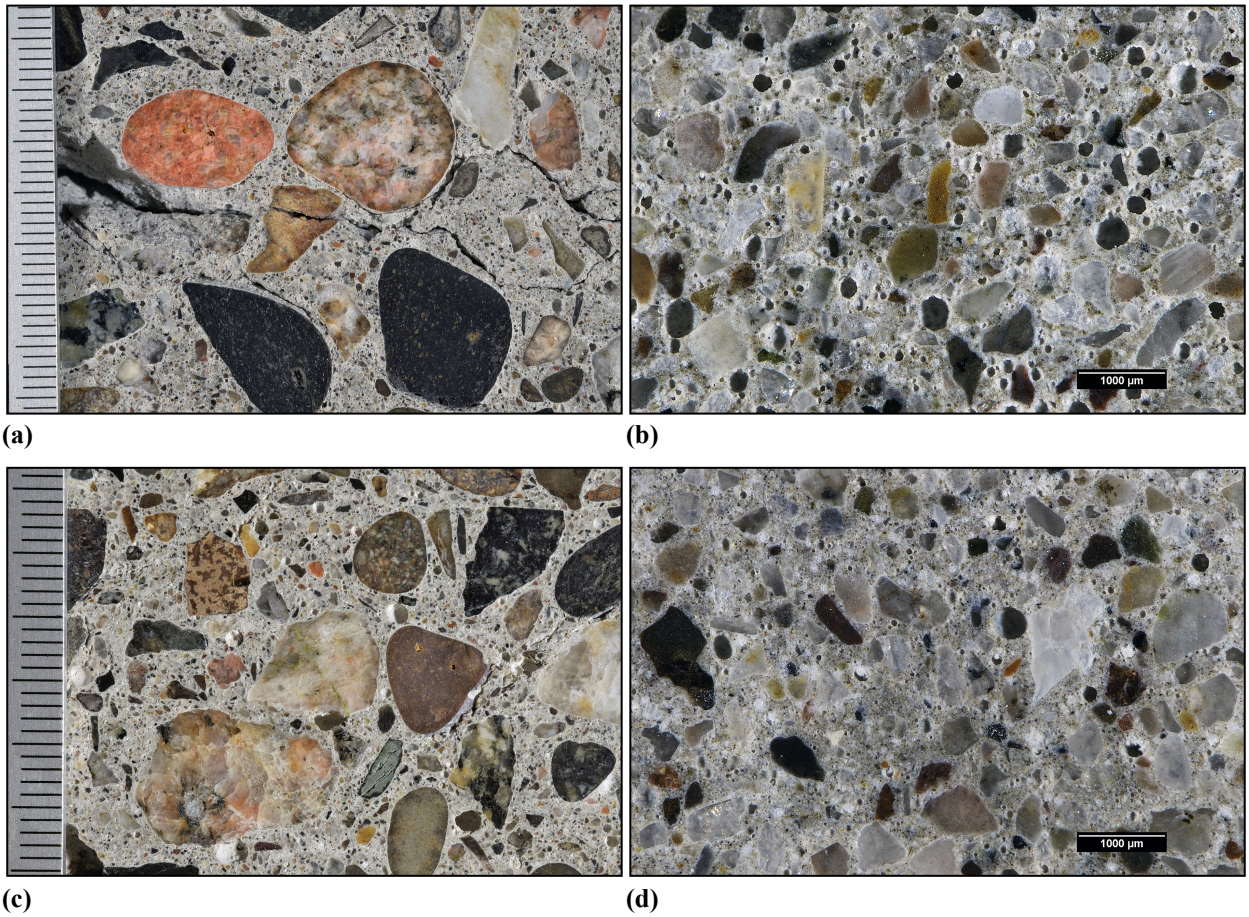

(a) (b)

(c) (d)

Figure 7. (a) Photograph and (b) reflected light photomicrograph of polished surface of Sample 2 showing coarse and fine aggregate, respectively. (c) Photograph and (d) reflected light photomicrograph of polished surface of Sample 5 showing coarse and fine aggregate, respectively. The scale is in millimeters in (a) & (c).

3.5 *Cracking & Microcracking*

Both of the cores show extensive cracking and microcracking across the full length of the cores. Three cracking mechanisms were observed.

Early age shrinkage cracking Linear cracks were observed cutting sub-vertically from the top surface to depths that reach 25 mm (1 in.) in both cores. These cracks range up to 750 µm (30 mil) wide; they mainly cut around aggregate particles and are mostly free of secondary deposits. Paste discoloration was also observed along the cracks in Sample 2 due to carbonation, which indicates the long presence of the crack. These linear cracks are likely due to drying shrinkage cracking. The early age cracks facilitate the moisture immigration and the occurrence of ASR, which is indicated by the minor deposits of ASR gel at the bottom end of the cracks. **Figure 8** shows examples of shrinkage cracks.

Freeze-thaw cracking Both cores show multiple sub-horizontal cracks throughout the entire depth of the cores. These cracks range up to 1 mm (40 mil) wide and commonly strike across the full width of the polished surface. These cracks mainly cut around aggregate particles and commonly show splays and bifurcations. The cracks are mostly free of secondary deposits but voids along the walls of the cracks commonly contain deposits of ettringite. These properties are consistent with freeze-thaw damage. Sample 2 shows more severe freeze-thaw damage than Sample 5. Occasionally the cracks cut through aggregate particles and contain minor deposits of ASR gel. **Figure 9** shows examples of typical freeze-thaw cracks in both cores.

Alkali-silica reaction cracking Both cores show evidence of pattern cracking and microcracking due to ASR. The cracking and microcracking is present through the full length of both cores up to 50-55 mm (2 - 2 ¼ in.) long and 200 µm (8 mil) wide. These cracks commonly cut through or radiate from aggregate particles and contain ASR gel. These cracks due to ASR are finer than the sub-horizontal cracks due to freeze-thaw damage and they are commonly terminated by the cracks due to freeze-thaw damage. This indicates ASR damage occurred after the presence of freeze-thaw damage. Microcracks ranging up to 100 µm (4 mil) wide and 40 mm (1 ½ in.) long were observed in both cores. These microcracks radiate from reactive aggregate particles or cut through aggregate particles. They commonly contain deposits of ASR gel. **Figure 10** shows examples of cracks and microcracks associated with ASR

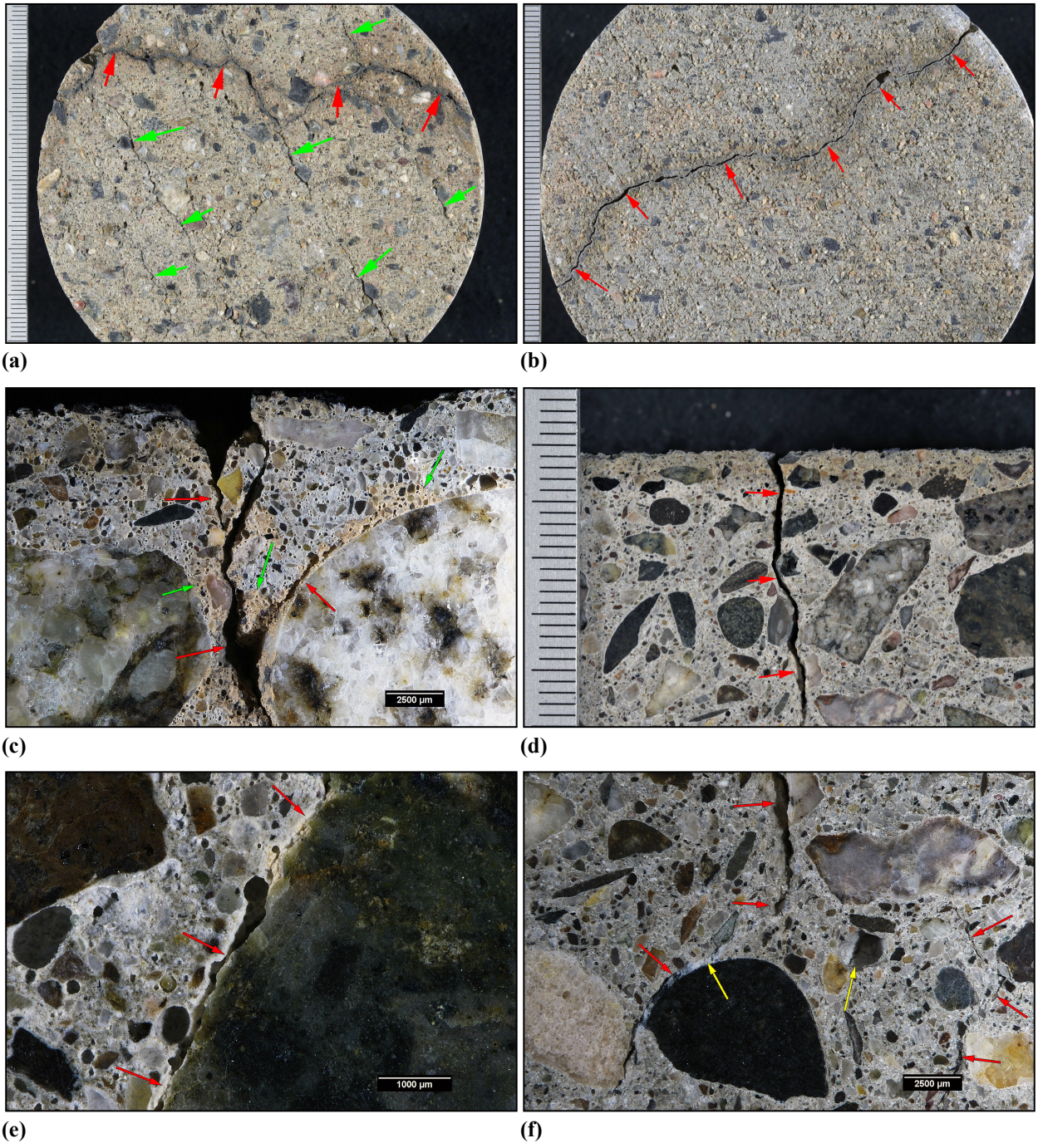

Figure 8. Photographs of the top surface of (a) Sample 2 and (b) Sample 5, respectively, showing overview of linear orthogonal cracks (red/green arrows) on the top of the core; scale in millimeters. (c) Photograph of the polished surface of Sample 2 showing the sub-vertical cracks (red arrows) near the top of the core. The green arrows indicate paste discoloration due to carbonation. (d) Reflected light photomicrograph of the polished surface of Sample 5 showing the sub-vertical cracks (red arrows) near the top of the core. Photographs of (e)-(f) Reflected light photomicrograph of the polished surface of (e) Sample 2 and (f) Sample 5 showing the bottom end of the cracks (red arrows) filled with ASR gel (yellow arrows).

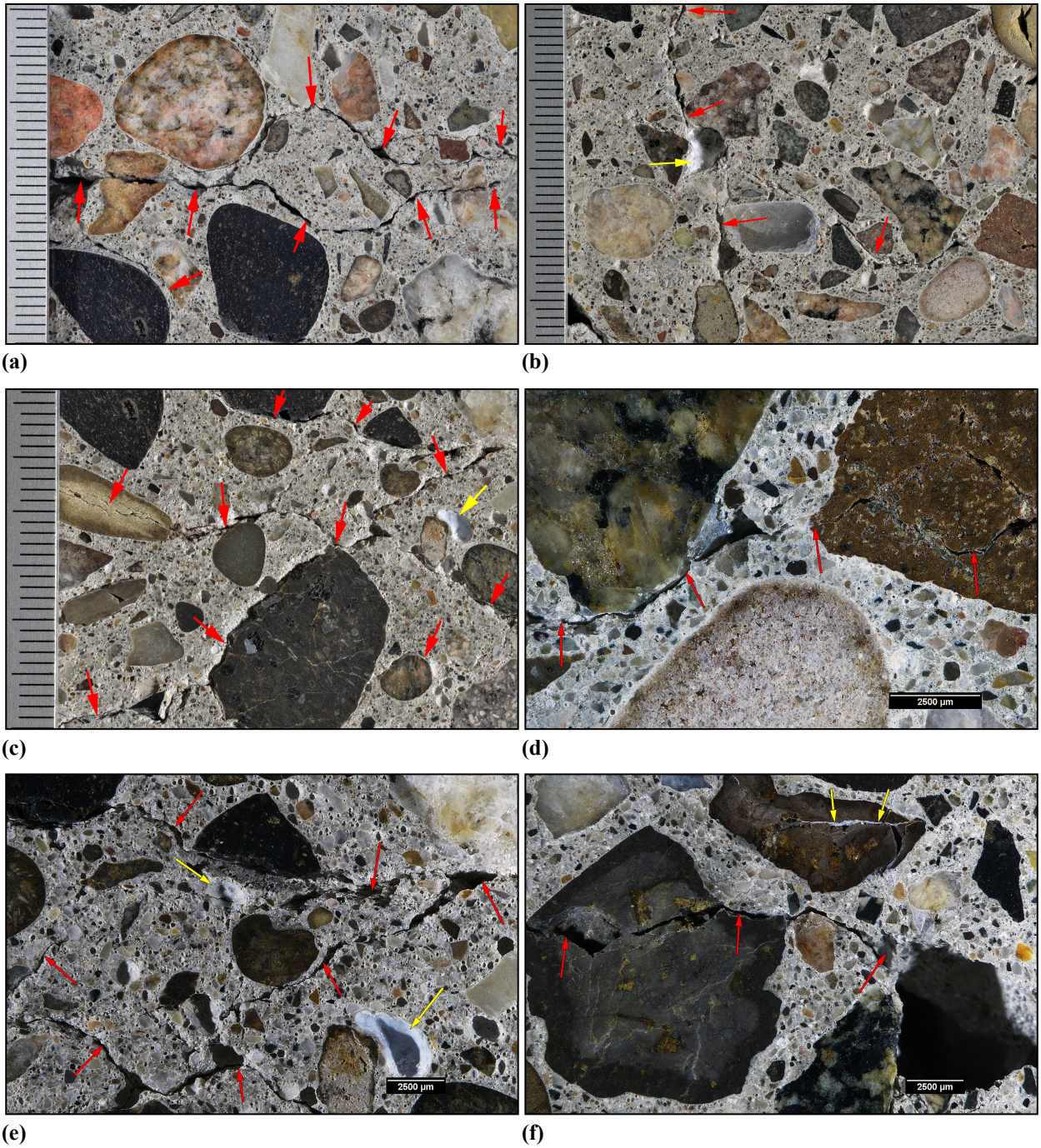

Figure 9. Photographs and photomicrographs of the polished surface of Sample 2 and Sample 5 showing the sub-horizontal cracks (red arrows). (a), (c) and (e): Sample2. (b), (d) and (f): Sample 5. The yellow arrow indicate deposits of ASR gel. The scale in (a)-(c) is in millimeters.

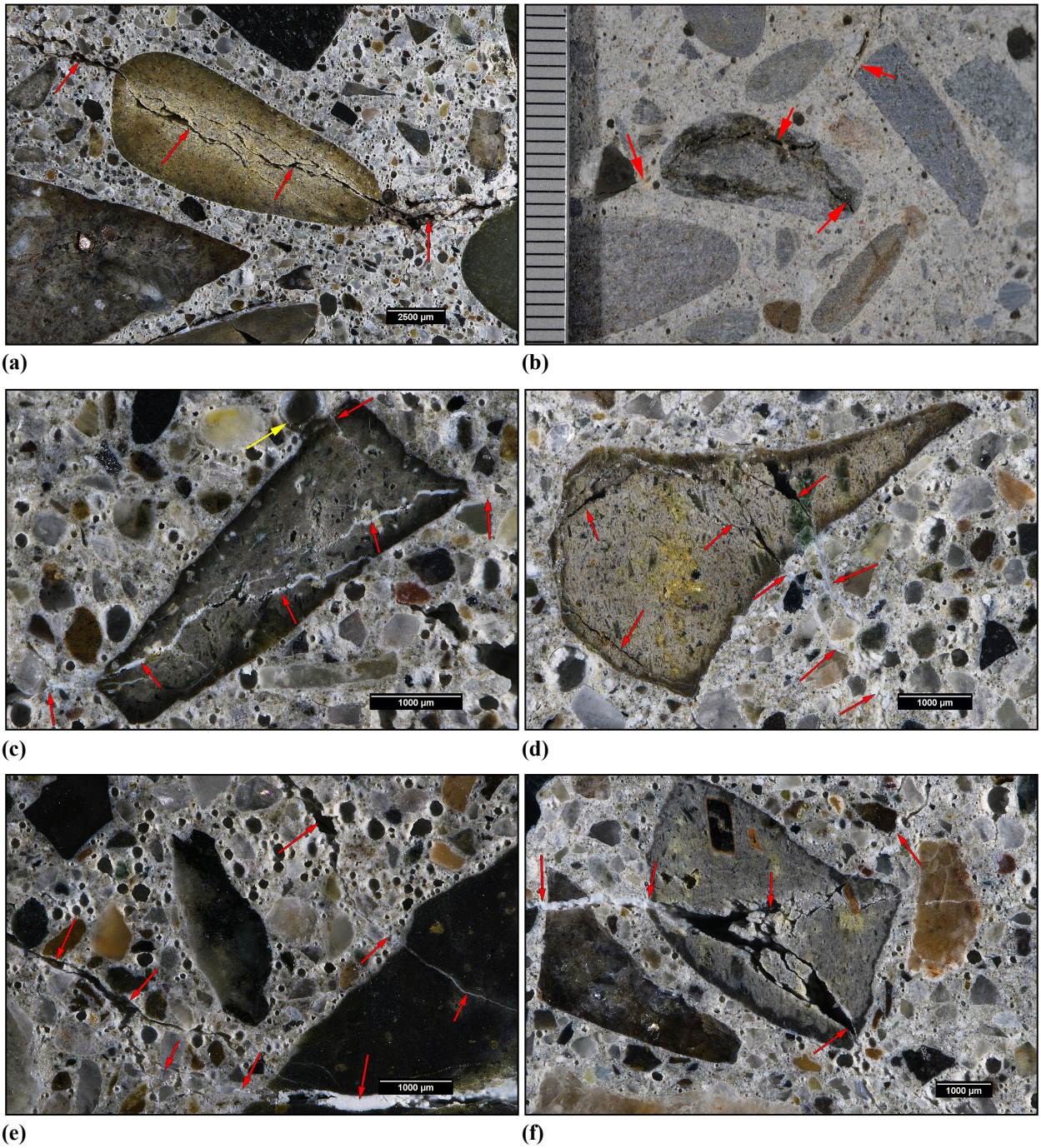

(a) (b)

(c) (d)

(e) (f)

Figure 10. (a) Reflected light photomicrograph of the polished surface of Sample 2 showing a crack (red arrows) cutting through a rhyolite particle in the middle of the core. (b) Photograph of the side of Sample 5 showing overview of cracks (red arrows) radiating from an aggregate particle; scale in millimeters. (c)-(f) Reflected light photomicrographs of the polished surface of Sample 2 and Sample 5 showing microcracks (red arrows) radiating from and cutting through aggregate particles. (c)&(e): Sample 2. (d)&(f): Sample 5. The aggregate particles in (c), (d) and (f) are rhyolite, while the particle in (e) is andesite.

3.5 *Secondary Deposits*

Carbonation Carbonation is negligible except for ~ 2 mm (80 mil) from the top of Sample 5. Sample 2 does not show evidence of significant carbonation except for occasional carbonation along the walls of the sub-vertical cracks near the top of the core.

Ettringite Deposits of ettringite were observed commonly in voids throughout both cores. Some fine voids are filled up with ettringite, especially along the sub-horizontal cracks. The deposits of ettringite indicate the concrete represents by the cores was exposed to high levels of moisture for a prolonged time. While there is not evidence of internal expansion associated with the deposits that led to cracking, the ettringite is significant from a durability standpoint. The filling of voids with ettringite appears to have diminished the freeze-thaw resistance of the concrete and the abundance of ettringite demonstrates the concrete had elevated levels of internal relative humidity that facilitates the progression of ASR.

Alkali-Silica Reaction Deposits of ASR gel were observed around aggregate particles, in cracks/microcracks and in voids throughout both cores. The ASR is rated as severe for both cores based on a subjective rating scale developed by DRP. **Table 2** summarizes this scale. The ASR is rated at Stage V using an evaluation scheme described by Katayama et al. [**1**]. **Table 3** describes this rating scheme. **Figure 11** shows examples of typical reactive aggregate particle in the cores.

The reactive components observed in the present cores include rhyolite, quartzite, chert and andesite most commonly in coarse aggregate and occasionally fines. The ASR is most commonly associated with particles in coarse aggregate in both core.

Table 2. DRP criteria for severity of ASR damage

Severity	Criteria
Absent	No reaction rims, microcracks or cracks associated with ASR
Negligible	Only reaction rims observed
Trace	ASR gel rarely observed lining voids near aggregate particles
Minor	ASR gel in voids near reactive particles or rimming reactive particles; microcracks with ASR gel rarely to occasionally observed
Moderate	Microcracks filled with ASR gel commonly observed
Severe	Cracks (> 100 µm wide) due to ASR observed

Table 3. Petrographic stages of ASR (after [1])

Stage	Criteria
I	Formation of reaction rims within aggregate particles.
II	Exudation of ASR sol/gel around aggregate particles. Darkening of paste around aggregate particles.
III	Cracking of aggregate; ASR gel may line or fill crack.
IV	Propagation of cracks from reacted aggregate into paste. ASR gel may line or fill crack; crack width grows.
V	Filling/lining of ASR gel into distant air voids. Note crack width for advanced damage.

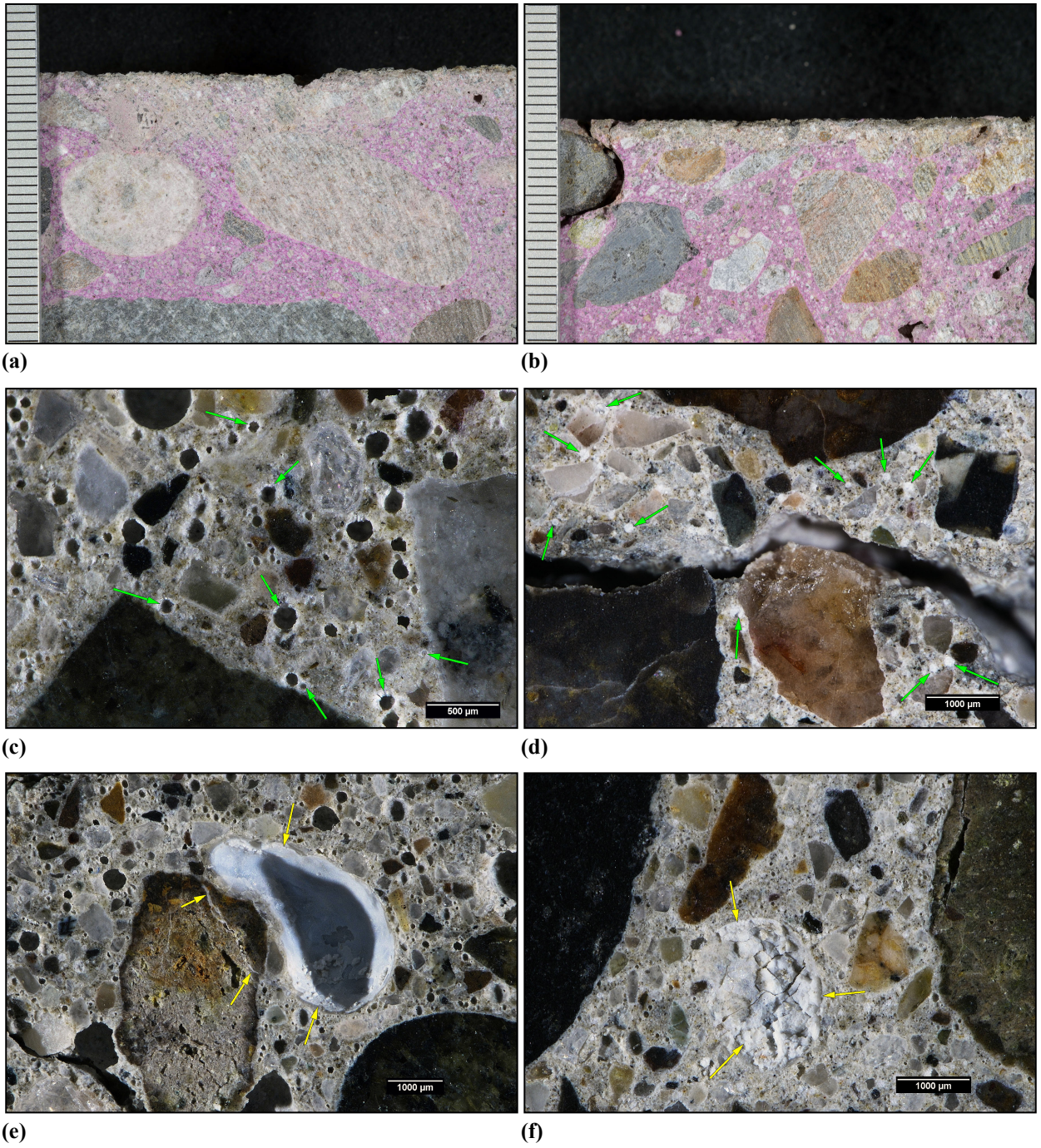

Figure 11. (a)-(b) Photographs showing detail of phenolphthalein-stained surface of (a) Sample 2 and (b) Sample 5, respectively, near the top of the cores; scale in millimeters. (c)-(d) Reflected light photomicrographs of the polished surface of Sample 2 and Sample 5, respectively, showing overview of entrained air voids filled with ettringite (green arrows). (e)-(f) Reflected light photomicrographs of the polished surface of Sample 2 and Sample 5, respectively, showing overview of ASR gel (yellow arrows) lining voids in the middle of the cores.

4.0 CONCLUSIONS

The findings described above indicate that there is clear evidence of ASR in the concrete represented by both cores. The ASR is rated as severe and is associated with internal expansion and cracking. However, ASR is not the only cracking mechanism identified in the cores. Three distinct mechanisms are present as follows.

- Early age cracks that are up to 750 µm (30 mil) wide which cut sub-vertically up to 25 m (1 in.) from the top surface. These cracks mainly cut around aggregate particles and are mostly free of secondary deposits but occasionally show evidence of carbonation along their walls. These cracks are typical of early age drying shrinkage. They are significant from a durability perspective because they facilitate the ingress of moisture which is associated with both freeze-thaw damage and alkali-silica reaction (ASR).
- Sub-horizontal cracks that range up to 1 mm (40 mil) wide cut across the full width of both cores. These cracks mainly cut around aggregate particles and show occasional splays and bifurcations. Deposits of ettringite were observed in voids along the walls of the cracks. These characteristics are typical of cracking due to freeze-thaw damage. Sample 2 shows more severe freeze-thaw damage compared to Sample 5. While the deposits of ettringite are not associated with an internal expansion mechanism associated with the observed cracking, they indicate high levels of moisture along the walls of the cracks. Filling of voids with ettringite may also increase the susceptibility of the concrete to freeze-thaw damage. Segments of these cracks occasionally cut through aggregate particles and contain minor deposits of ASR gel.
- Cracking and microcracking from alkali-silica reaction (ASR) was observed commonly in both cores. These cracks range up to 50-55 mm (2 - 2 ¼ in.) long and 200 µm (8 mil) wide. These cracks and microcracks are filled with ASR gel and radiate outward from or cut through reactive aggregate particles. The cracks and microcracks are interconnected and form complex networks of cracks and microcracks. Cracks due to ASR are more narrow than the sub-horizontal cracks due to freeze-thaw damage. They commonly cut into cracks associated with freeze-thaw damage, indicating that at least some ASR damage occurred after the presence of freeze-thaw damage. Some examples of mutually cross-cutting relationships between cracks associated with ASR and freeze-thaw damage indicate that both mechanisms also operated coevally.

Both cores contain coarse aggregate that consists of a siliceous gravel. The reactive components present in the aggregate include rhyolite, quartzite, chert and andesite. Reactive particles are observed most commonly in the coarse and occasionally in the fine aggregate. The ASR is at Stage V using a qualitative scale described by Katayama et al. [**1**] and is severe using a qualitative scale described by DRP.

Table C1. DRP criteria for severity of ASR damage

Severity	Criteria
Absent	No reaction rims, microcracks or cracks associated with ASR
Negligible	Only reaction rims observed
Trace	ASR gel rarely observed lining voids near aggregate particles
Minor	ASR gel in voids near reactive particles or rimming reactive particles; microcracks with ASR gel rarely to occasionally observed
Moderate	Microcracks filled with ASR gel commonly observed
Severe	Cracks (> 100 µm wide) due to ASR observed

Table C2. Petrographic stages of ASR (after [1])

Stage	Criteria
I	Formation of reaction rims within aggregate particles.
II	Exudation of ASR sol/gel around aggregate particles. Darkening of paste around aggregate particles.
III	Cracking of aggregate; ASR gel may line or fill crack.
IV	Propagation of cracks from reacted aggregate into paste. ASR gel may line or fill crack; crack width grows.
V	Filling/lining of ASR gel into distant air voids. Note crack width for advanced damage.

The cores represent concrete mixtures that are similar except for the composition of the paste and the nominal top size of the aggregate. In Sample 2 the paste contains hydrated portland cement with no fly ash, slag cement or other supplemental cementitious materials observed. In Sample 5 the paste contains portland cement and fly ash; no slag cement of other supplemental cementitious materials observed. The coarse aggregate is a crushed siliceous gravel with a 25 mm (1 in.) nominal top size in Sample 2 and a 19 mm (¾ in.) nominal top size in Sample 5. The coarse aggregate is siliceous in composition and consists primarily of rhyolite, granitic rocks, quartzite and chert with minor andesite and basalt. The fine aggregate is a natural sand that consists of rocks similar to those in the coarse aggregate. Both cores are air entrained with ~ 6% estimated total air content.

This concludes work performed on this project to date.

David Rothstein, Ph.D., P.G., FACI
Principal Petrographer

Chunyu (Joe) Qiao, Ph.D.
Senior Petrographer

Billings Logan International Airport Aprons Core Petrography

Appendices

Appendix A	**Sample 2 Petrography (ASTM C856)**
Appendix B	**Sample 5 Petrography (ASTM C856)**
Appendix C	**Procedures**

1. Received Condition	
Orientation & Dimensions	Vertical core extracted from a bridge deck measures ~ 95 mm (3 ¾ in.) in diameter and is 160 – 205 mm (6 ¼ – 8 in.) long (**Figure A1, Figure A2**).
Surfaces	The top surface is worn and expose coarse aggregate particles (**Figure A3**) and the bottom surface is a fracture such that the core represents a partial thickness of the bridge deck.
General Condition	The concrete is hard and compact and rings lightly when sounded with a hammer. A sub-horizontal crack ~ 120 mm (4 ¾ in.) below the top surface cuts the core into two pieces. Because the crack is open the original width cannot be measured. White deposits of ASR gel were observed lining voids and coarse aggregate particles on the fracture surface and the bottom surface (**Figure A4**).

2. Embedded Objects	
General	None observed.

3. Cracking	
Macroscopic	A linear crack measuring ~ 60 mm (2 ⅜ in.) long and 200 – 300 µm (8 – 12 mil) wide strike across the top of the core (**Figure A5**). It cuts sub-vertically to 15 – 25 mm (⅝ – 1 in.) from the top of the core, passing mainly around coarse aggregate particles. ASR gel fills the crack at the bottom. Additional parallel cracks were also observed on the top of the core. They measure up to 50 mm (2 in.) long and 100 – 500 µm (4 – 20 mil) wide. They sub-vertically cut to ~ 30 mm (1 ¼ in.) from the top. They mainly cut around aggregate particles and are partially filled with ASR gel. As described above, a sub-horizontal crack cuts the core in two ~ 120 mm (4 ¾ in.) from the top surface. Multiple additional sub-horizontal cracks were observed throughout the entire depth of the core. They sub-vertically strike across the core. They measure up to 95 mm (3 ¾ in.) long and 1 mm (40 mil) wide and occasionally show splays and bifurcations. The cracks cut through several coarse aggregate particles and are partially filled with ASR gel. Additional relatively fine sub-vertical and sub-horizontal cracks were observed throughout the entire depth of the core. The cracks and microcracks are interconnected and form complex networks of cracking. They measure up to 55 mm (2 ¼ in.) long and up to 200 µm (8 mil) wide. They commonly cut throughout and radiate from aggregate particles and are filled with ASR gel.
Microscopic	Numerous microcracks were observed throughout the entire core (**Figure A6**). The microcracks are mainly sub-horizontal in orientation and form an interconnected network. The microcracks measure up to 40 mm (1 ⅜ in.) long and up to 100 µm (4 mil) wide. They occasionally to commonly cut through aggregate particles and are filled with ASR gel.

4. Voids	
Void System	Concrete is air-entrained and contains ~ 6% total air as estimated from visual and microscopical observations (not measured in accordance with ASTM C457; **Figure A7**). Most of the air voids are smaller than 200 µm (8 mil) across. The concrete is well consolidated.
Void Fillings	Ettringite was commonly observed lining voids throughout the entire core. ASR gel was occasionally observed lining and filling voids throughout the entire core.

5. Coarse Aggregate

Physical Properties	The coarse aggregate is a crushed gravel that has a 25 mm (1 in.) nominal top size (**Figure A8**). The rocks are hard and competent. The particles are sub-equant to slightly elongated with aspect ratios of 2:1. The particles have sub-angular to sub-rounded edges.
Rock Types	The aggregate is siliceous in composition and consist primarily of rhyolite with abundant phenocrysts of plagioclase and amphibole, granitic rocks, quartzite and chert. Minor amounts of andesite with abundant phenocrysts of amphibole and basalt were also observed. Abundant chlorite from hydrothermal alteration is present in rhyolite and granitic rocks. Rhyolite, granitic rocks, quartzite, chert and andesite are potentially susceptible to alkali-silica reaction (ASR).
Other Features	No deleterious coatings or incrustations observed. Low w/c mortar coatings were occasionally observed. Reaction rims were commonly observed. Internal cracking and microcracking were occasionally to commonly observed. Coarse aggregate particles occasionally show de-bounding. Deposits of ASR gel were commonly observed in internal cavities, microcracks radiating from it, de-bounding sockets and nearby voids.

6. Fine Aggregate

Physical Properties	The fine aggregate is a natural sand that consists of rocks that are hard and competent (**Figure A9**). The particles are mostly sub-equant to slightly elongated in shape with sub-rounded to sub-angular edges. The grading and distribution are relatively even.
Rock Types	The sand consists of siliceous rocks similar to that observed in coarse aggregate. The fines also contain fragments of quartz and chlorite. Rhyolite, granitic rocks, quartzite, chert and andesite are potentially susceptible to alkali-silica reaction (ASR).
Other Features	No deleterious coatings or incrustations observed. Internal microcracking and reaction rims were occasionally observed. Deposits of ASR were occasionally observed lining the microcracks and voids associated with fine aggregate particles.

7. Paste Observations

Polished Surface	Paste is light grey (2.5Y/7/1) and slightly mottled, has a smooth texture and a sub-vitreous luster (**Figure A10**). The paste is moderately hard (Mohs ~ 3.0).
Fresh Fracture	Fracture surface is light gray, has a granular texture and a sub-vitreous luster (**Figure A11**). The fracture dominantly cuts through ~ 50% of coarse aggregate particles. ASR gel was observed on the fracture surface.
Thin Section	The paste contains hydrated portland cement; no fly ash, slag cement or other SCM were observed. The hydration of the paste is normal with 4-8% RRCG that consist primarily of belite grains with interstitial aluminoferrite; alite was rarely observed and is very fine-grained with hydration rims (**Figure A12**). CH is fine grained and evenly distributed and makes up less than 4% of the paste.
Estimated w/cm	The capillary porosity of the paste is moderate and slightly heterogeneous (**Figure A13**). The estimated w/cm is not provided due to the elevated moisture level and secondary deposits.

** Abbreviations as follows: DSL = densified surface layer; RRCG = relict and residual cement grains; SCM = supplemental cementitious materials; CH = calcium hydroxide; ITZ = interfacial transition zone. Modal abundances are based on visual estimations.*

8. SECONDARY DEPOSITS	
PHENOLPHTHALEIN	Entire surface stains purple except for no staining occasionally along the sub-vertical crack from the top of the core (**Figure A14**).
SECONDARY DEPOSITS	Negligible carbonation was observed near the top of the core, while carbonation was observed occasionally along the sub-vertical crack from the top of the core. Deposits of gel were occasionally to commonly observed in voids and cracking/ microcracking throughout the entire depth of the core. Deposits of ettringite were observed commonly in voids throughout the entire depth of the core. ASR Rating: **Severe ASR**.

FIGURES

(a)

(b)

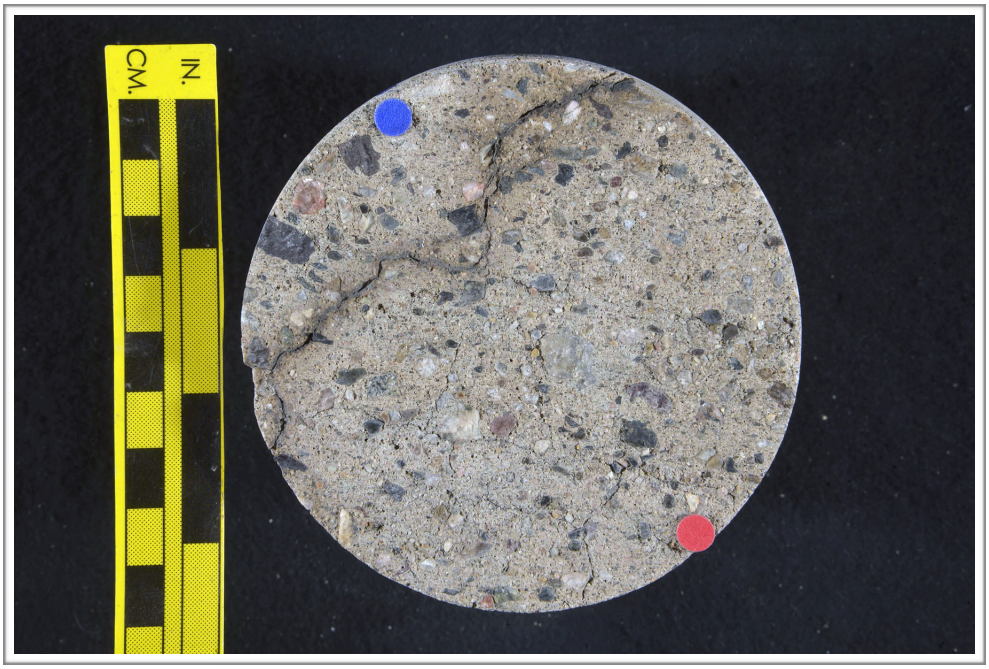

Figure A1. Photographs of the core in as-received condition showing (a) an oblique view of the top surface and side of the core with identification labels and (b) the top surface of the core. The red and blue dots show the orientation of the saw cuts used to prepare the core. The yellow scale is ~ 150 mm (6 in.) long; the small and large divisions are in centimeters and inches, respectively.

(c)

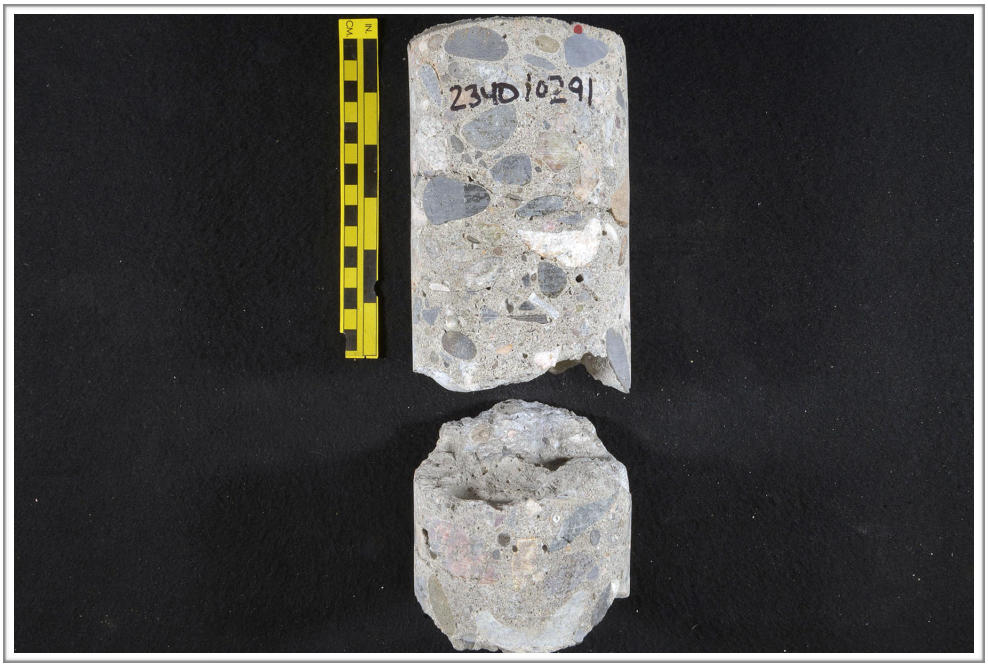

(d)

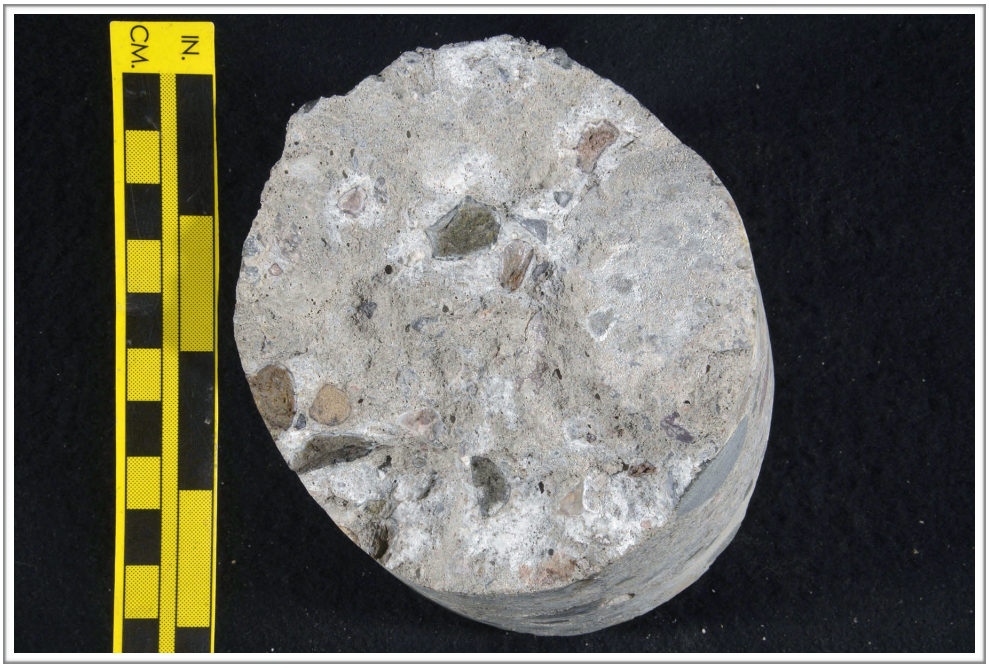

Figure A1 (cont'd). Photographs of the core in as-received condition showing (c) the side of the core and (d) the bottom surface of the core. The red and blue dots show the orientation of the saw cuts used to prepare the core. The yellow scale is ~ 150 mm (6 in.) long; the small and large divisions are in centimeters and inches, respectively.

Figure A2. Photograph showing the polished surfaces of the core. The small and large divisions on the yellow scale are in centimeters and inches, respectively.

(a)

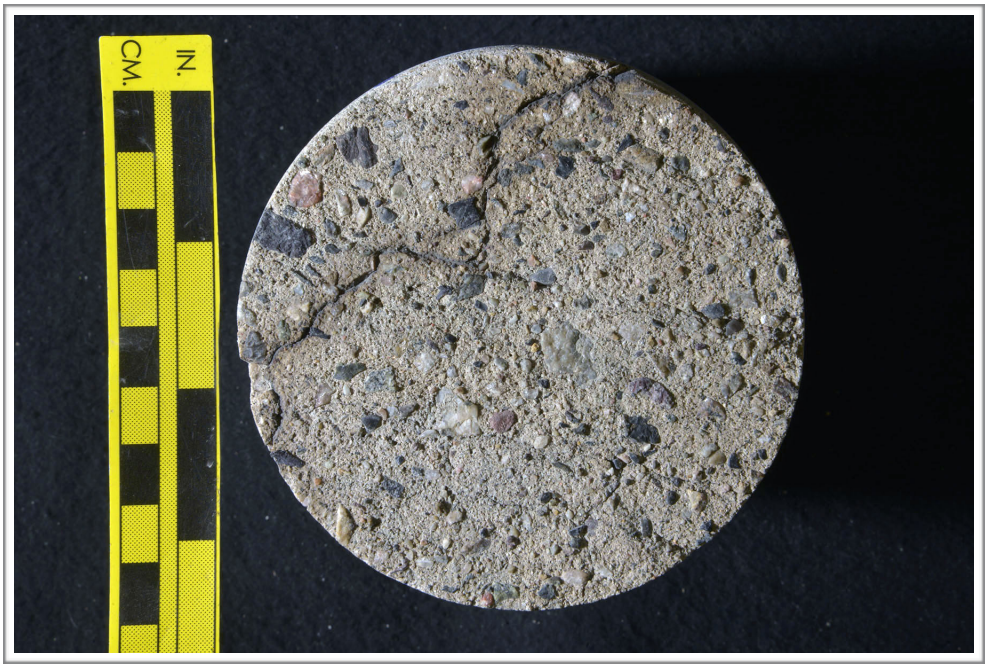

(b)

Figure A3. Photographs showing (a) overview and (b) detail of the top surface. The small and large divisions on the yellow scale in (a) are in centimeters and inches, respectively. The scale in (b) is in millimeters.

(a)

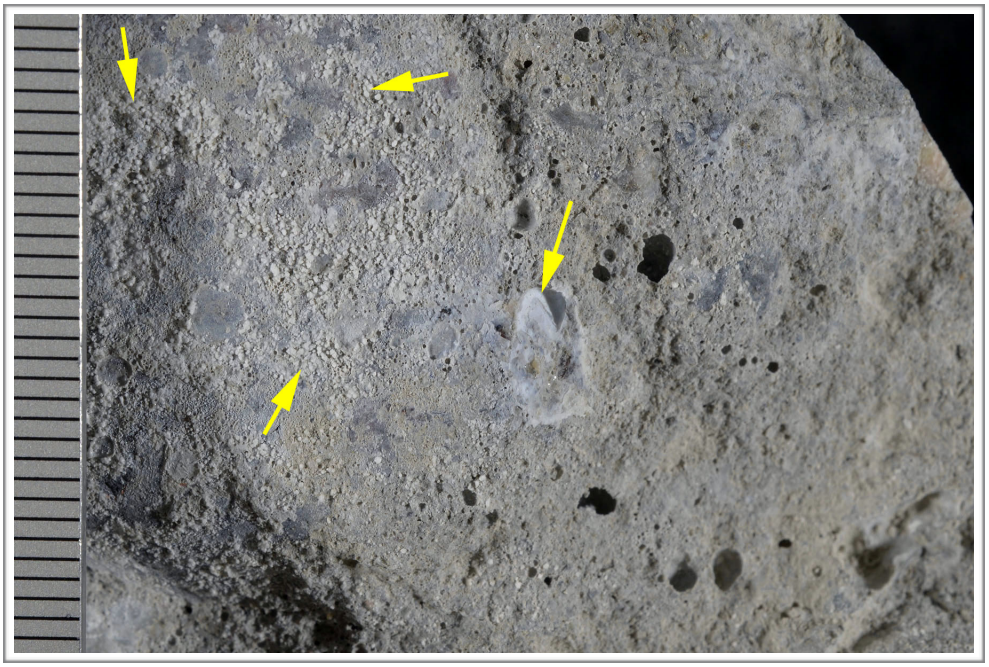

(b)

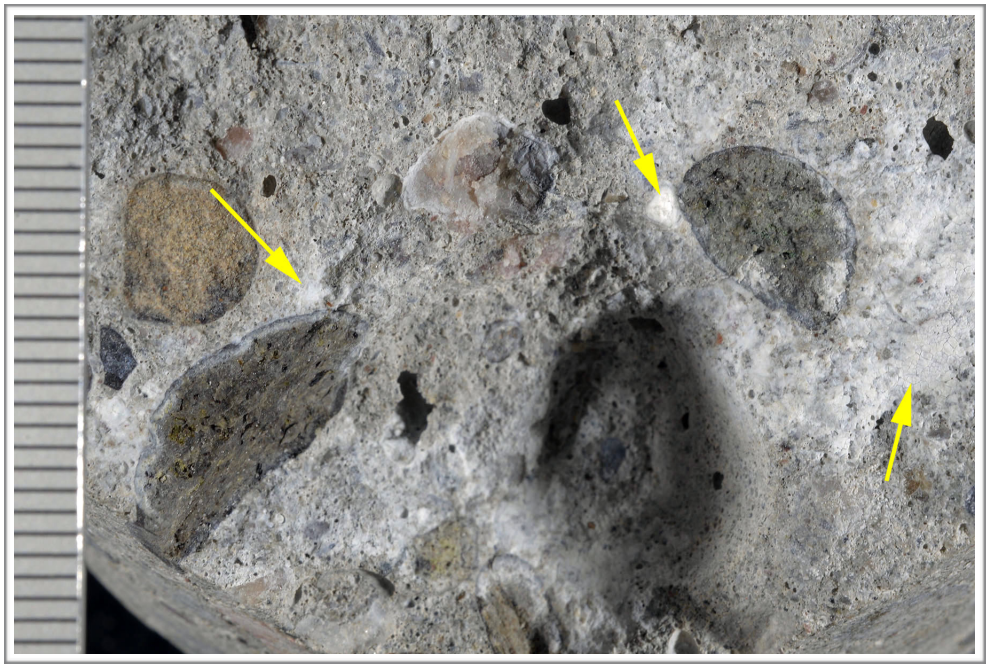

Figure A4. Photographs showing detail of ASR gel (yellow arrows) (a) on the fracture surface and (b) on the bottom surface of the core. The scale in two images is in millimeters.

(a)

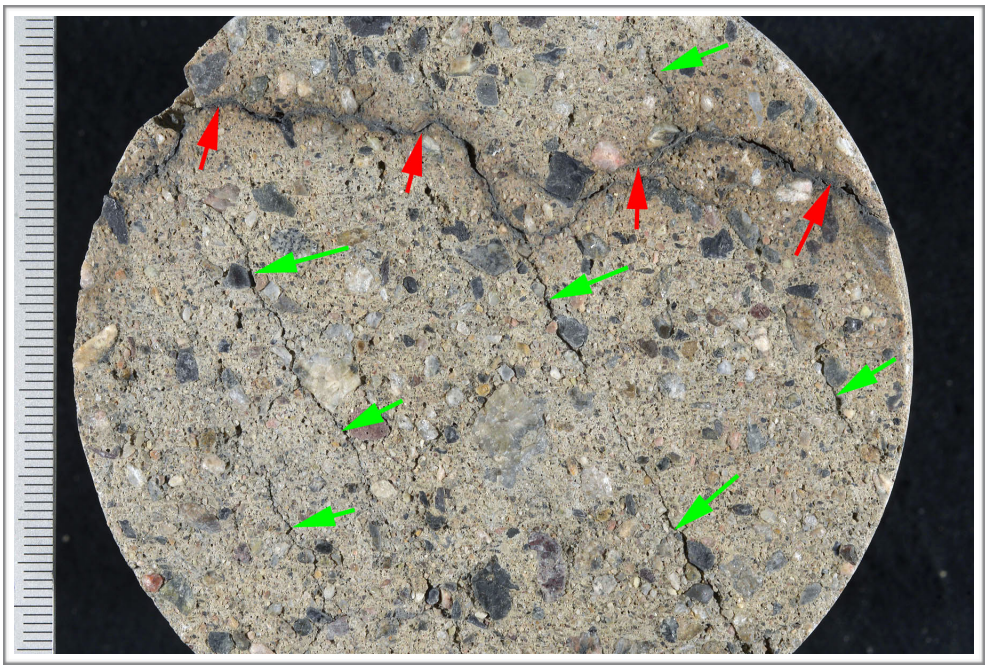

(b)

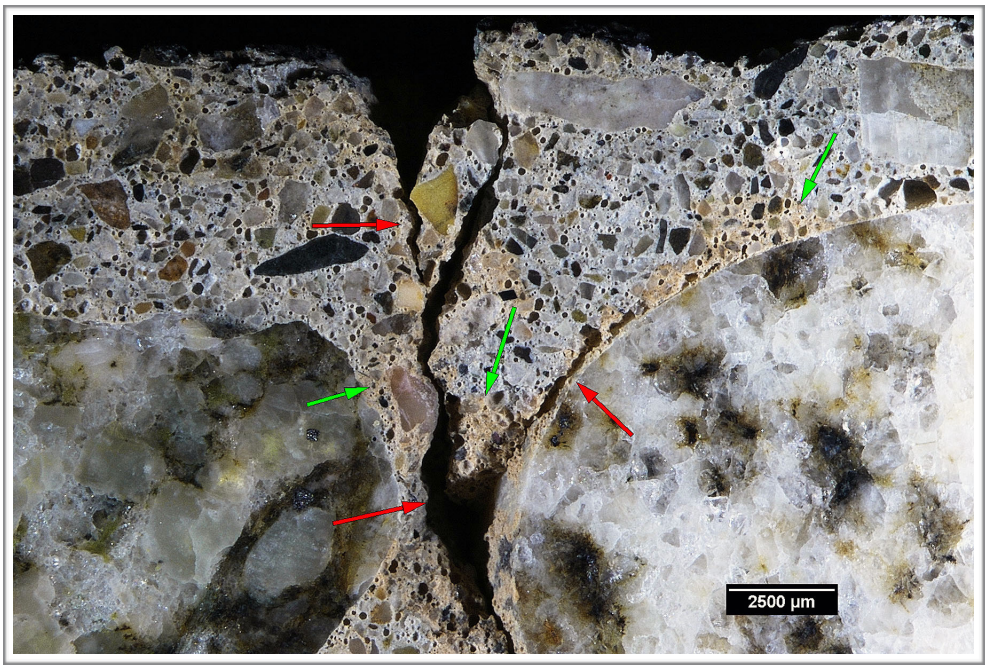

Figure A5. (a) Photograph of the top surface showing overview of the major crack (red arrows) and additional parallel cracks (green arrows); scale in millimeters. (b) Reflected light photomicrograph of the polished surface showing overview of the sub-vertical crack (red arrows) at the top of the core. The green arrows in (b) indicate paste discoloration due to carbonation.

(c)

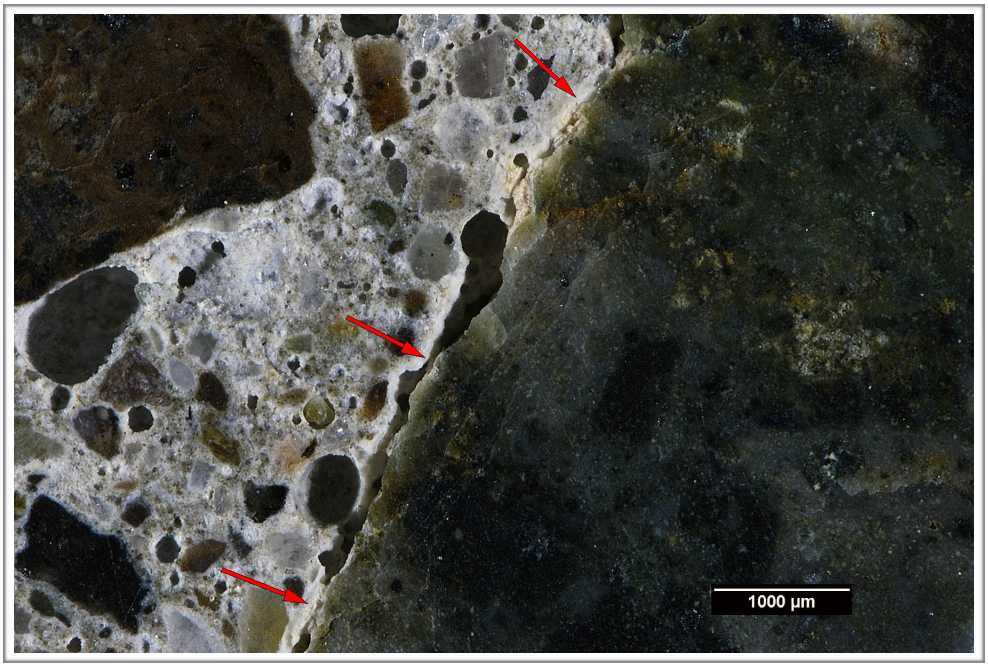

(d)

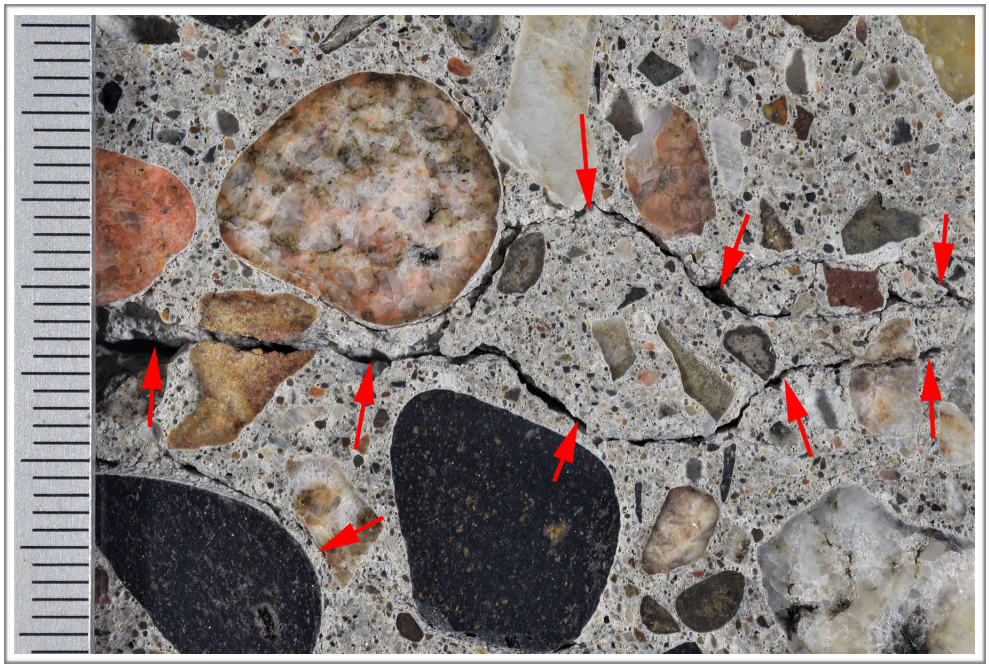

Figure A5 (Cont'd). (c) Reflected light photomicrograph of the polished surface showing detail of the crack (red arrows) with ASR gel at the bottom of the sub-vertical crack in (a). (d) Photograph of the polished surface showing overview of the sub-horizontal cracks (red arrows); scale in millimeters.

(e)

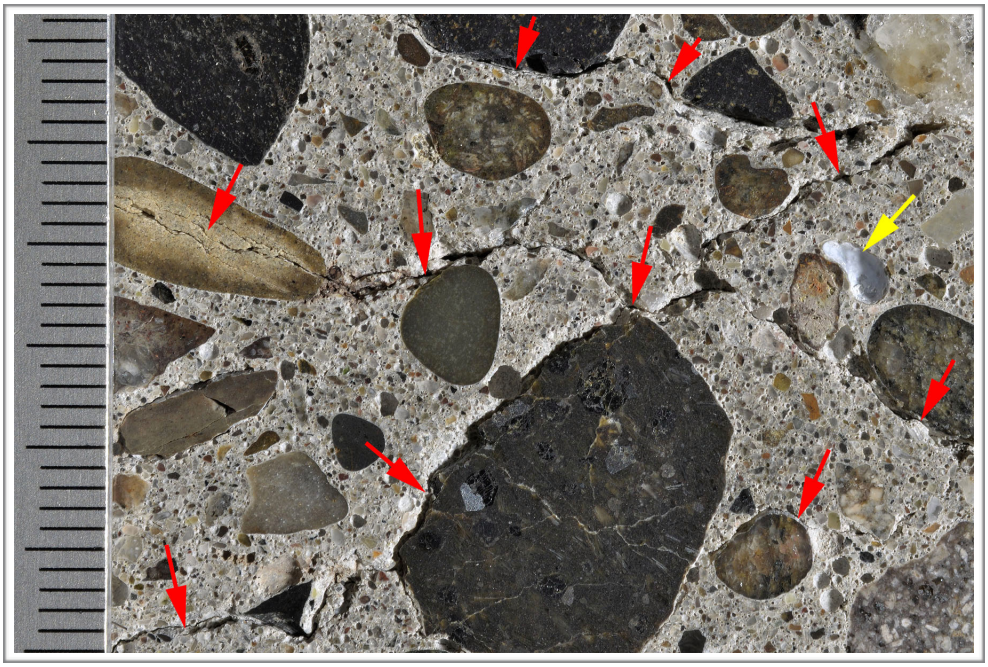

(f)

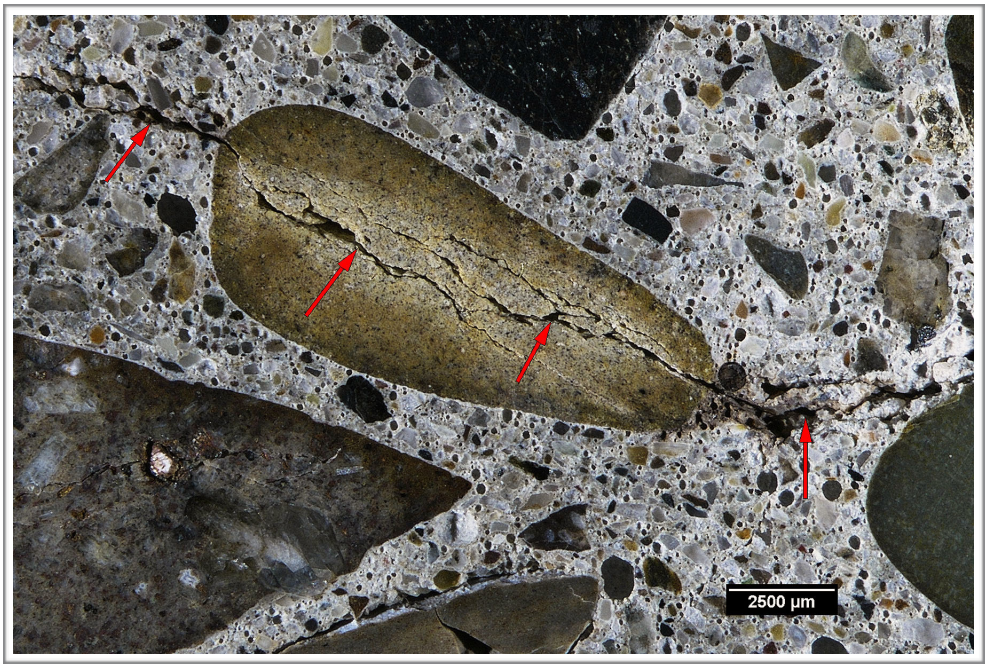

Figure A5 (Cont'd). (e) Photograph of the polished surface showing overview of the sub-horizontal cracks (red arrows); scale in millimeters. The yellow arrow in (e) indicates ASR gel in a void. (f) Reflected light photomicrograph of the polished surface showing overview of cracks (red arrows) cutting through a rhyolite particle. The yellow arrow in (f) indicates ASR gel lining the crack.

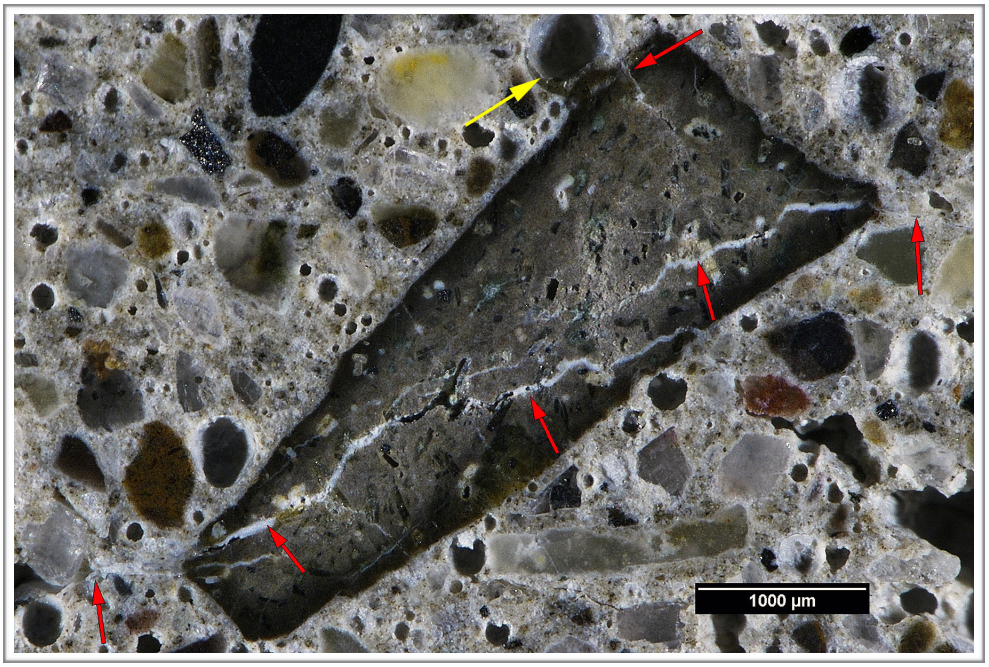

(a)

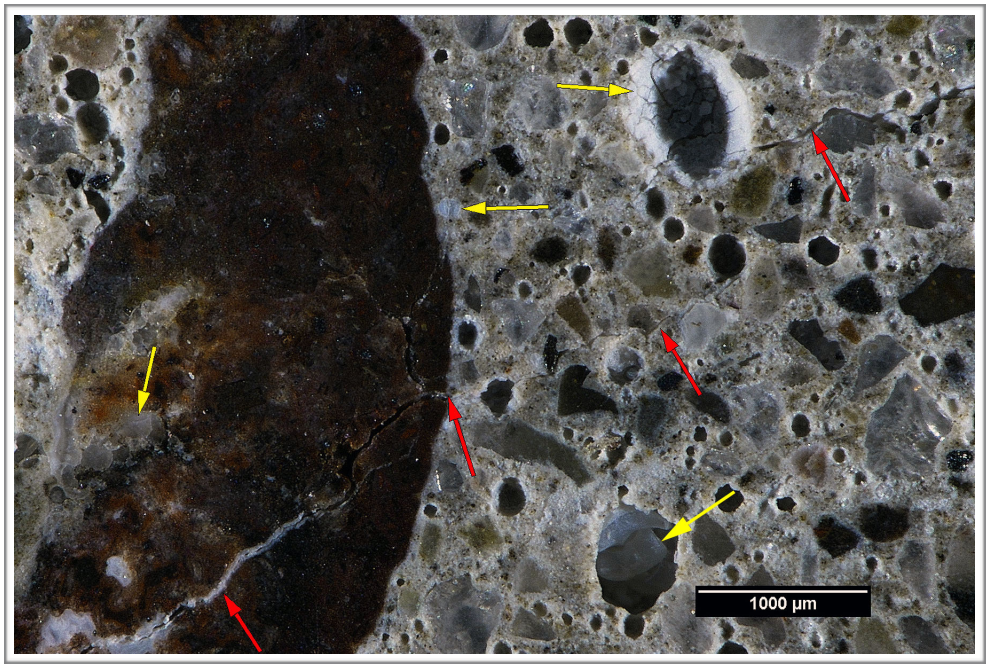

(b)

Figure A6. (a) Reflected light photomicrograph of the polished surface showing microcracks (red arrows) cutting through a rhyolite particle and filled with ASR gel. The yellow arrow in (a) indicates ASR gel lining a void. (b) Reflected light photomicrograph of the polished surface showing microcracks (red arrows) cutting through a rhyolite particle and filled with ASR gel. The yellow arrows in (a) indicates ASR gel lining voids and within the rhyolite particle.

(c)

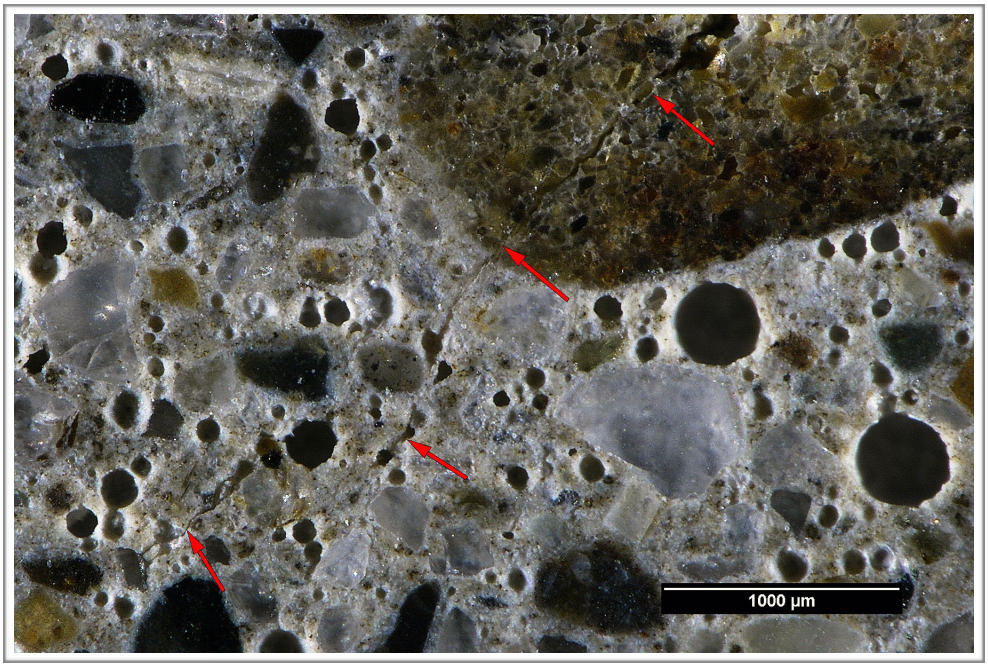

(d)

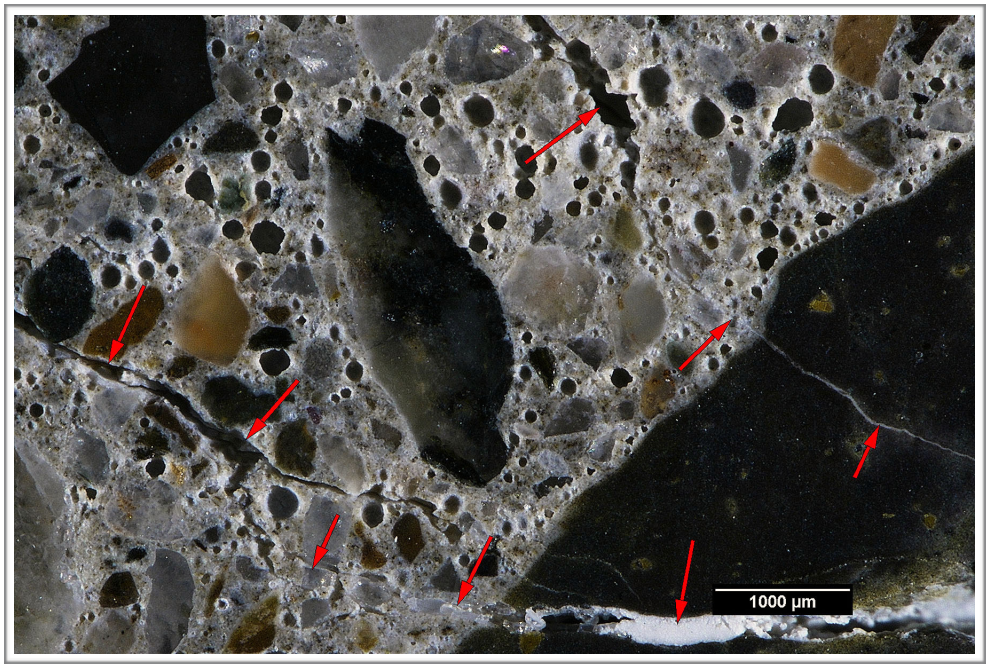

Figure A6 (Cont'd). (c) Reflected light photomicrograph of the polished surface showing microcracks (red arrows) cutting through a quartzite particle. (d) Reflected light photomicrograph of the polished surface showing microcracks (red arrows) cutting through an andesite particle and filled with ASR gel.

(a)

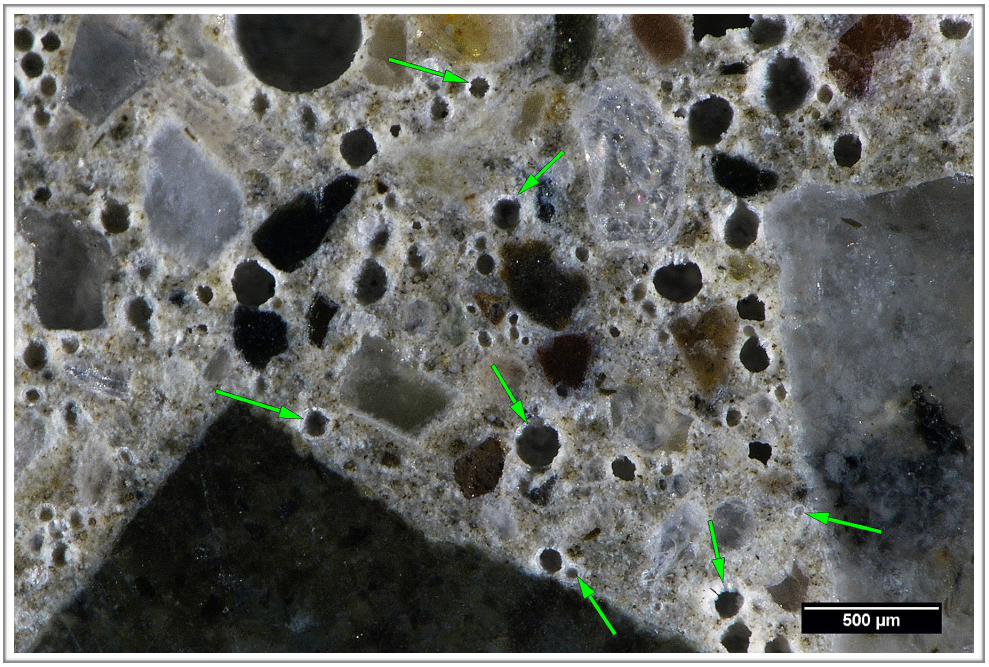

(b)

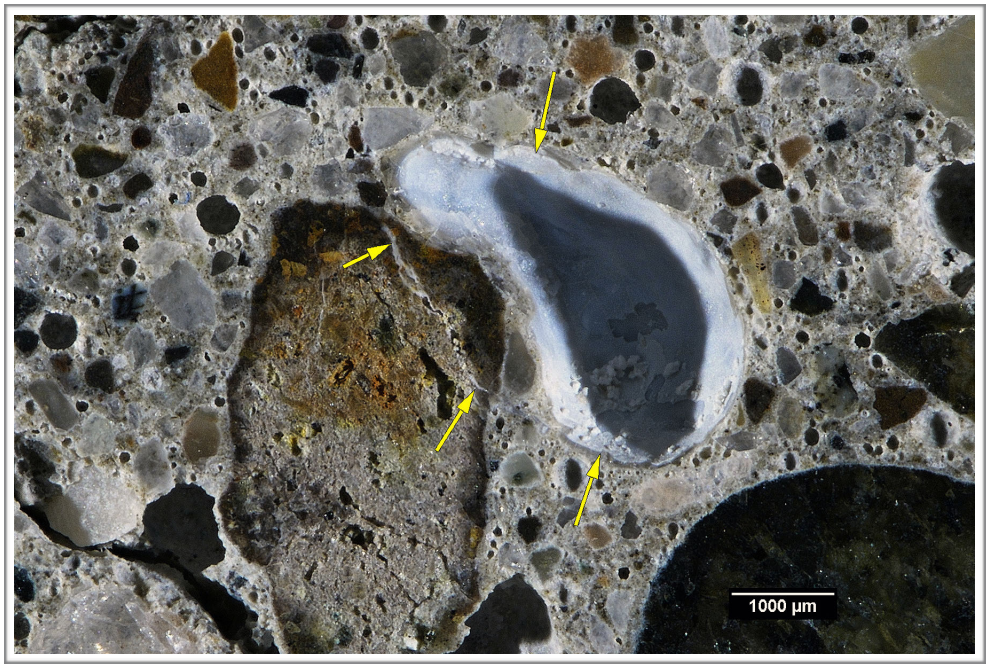

Figure A7. Oblique reflected light photomicrographs of the polished surface showing air voids filled with (a) ettringite (green arrows) and (b) ASR gel (yellow arrows) in the middle of the core.

(a)

(b)

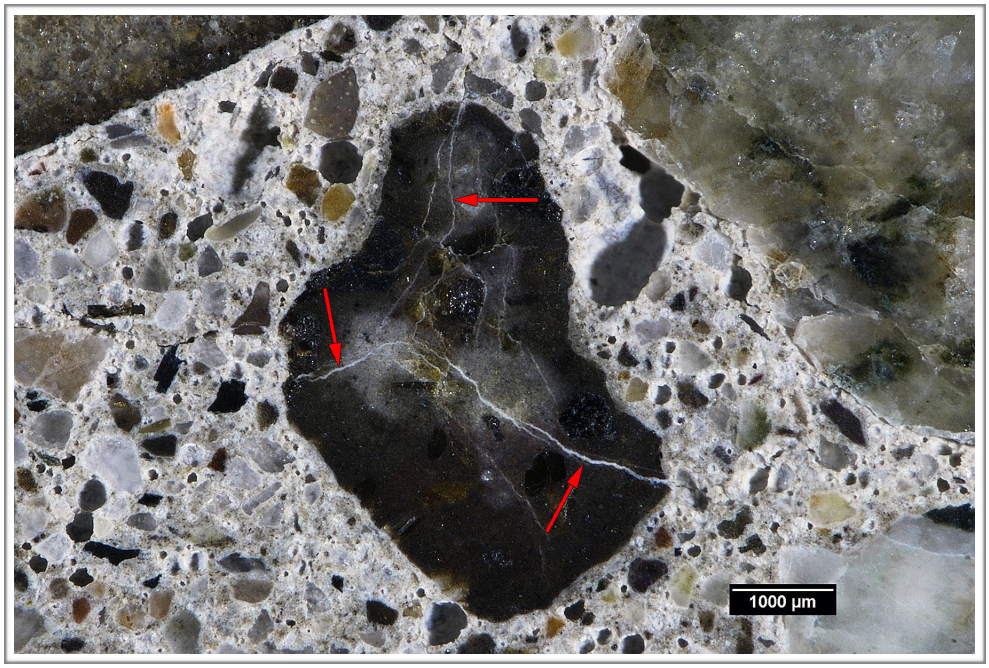

Figure A8. (a) Photograph of the polished surface showing overview of coarse aggregate; scale in millimeters. (b) Reflected light photomicrograph of the polished surface showing overview of a reacted andesite particle with internal microcracks filled with ASR gel (red arrows).

(a)

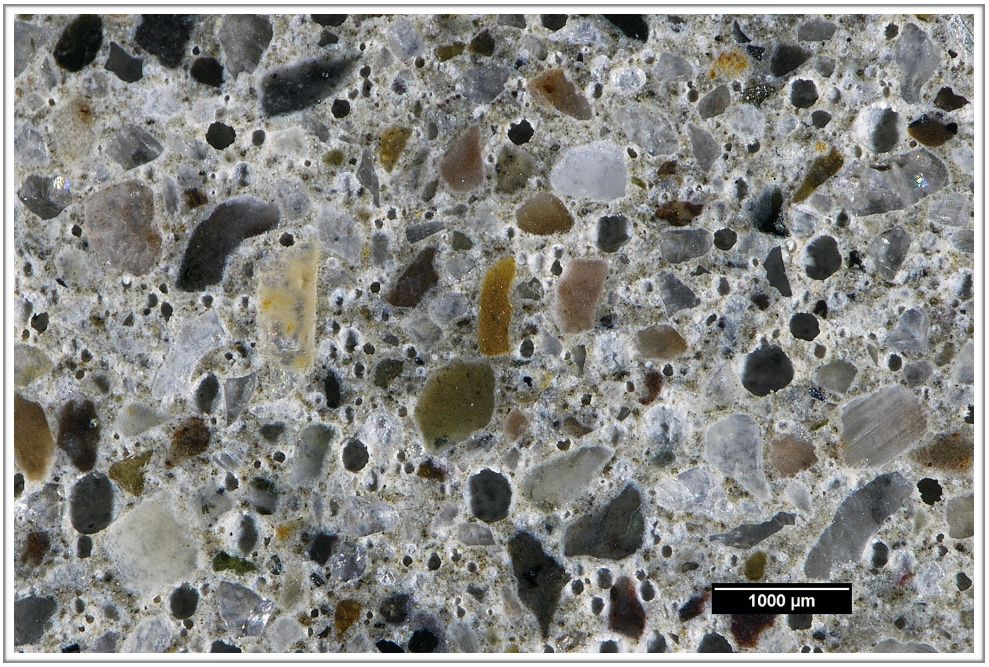

(b)

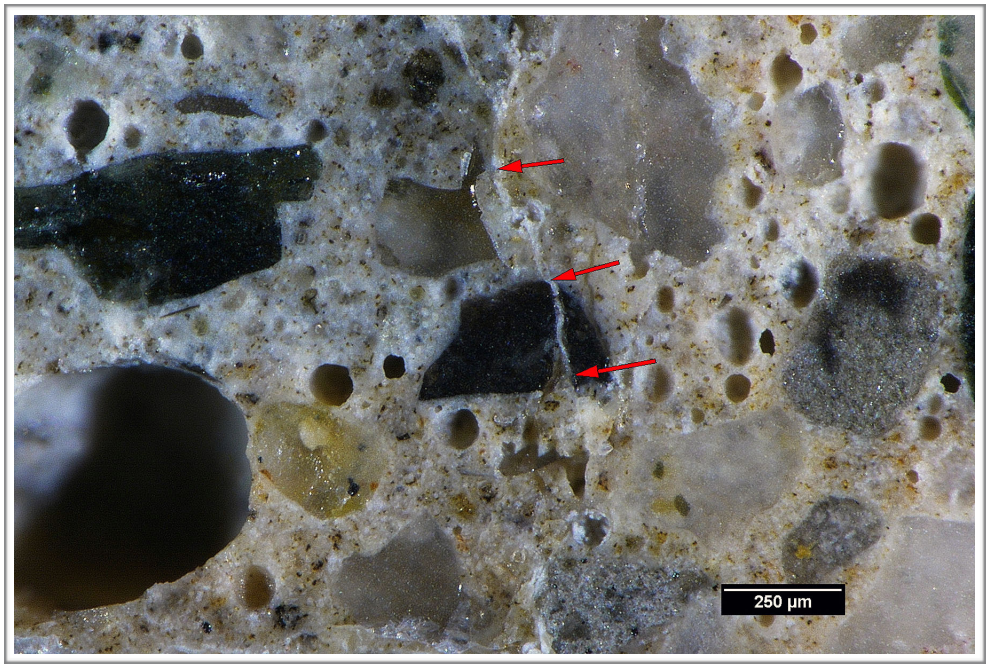

Figure A9. (a) Reflected light photomicrograph of the polished surface showing overview of the fine aggregate. (b) Reflected light photomicrograph of the polished surface showing overview of an andesite particle with microcracking (red arrows) with ASR gel cutting through it.

(a)

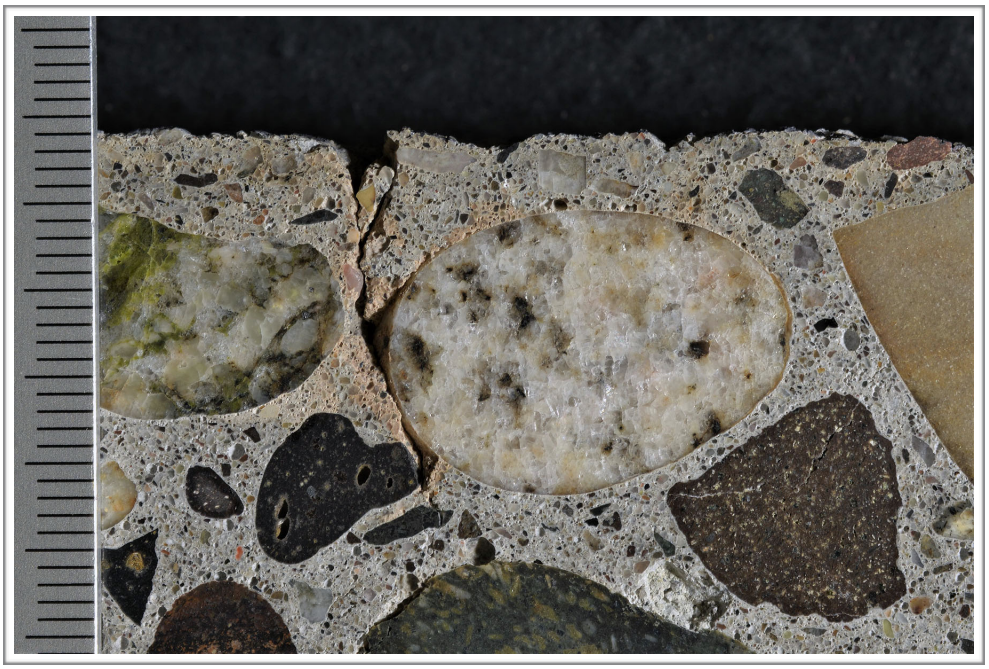

(b)

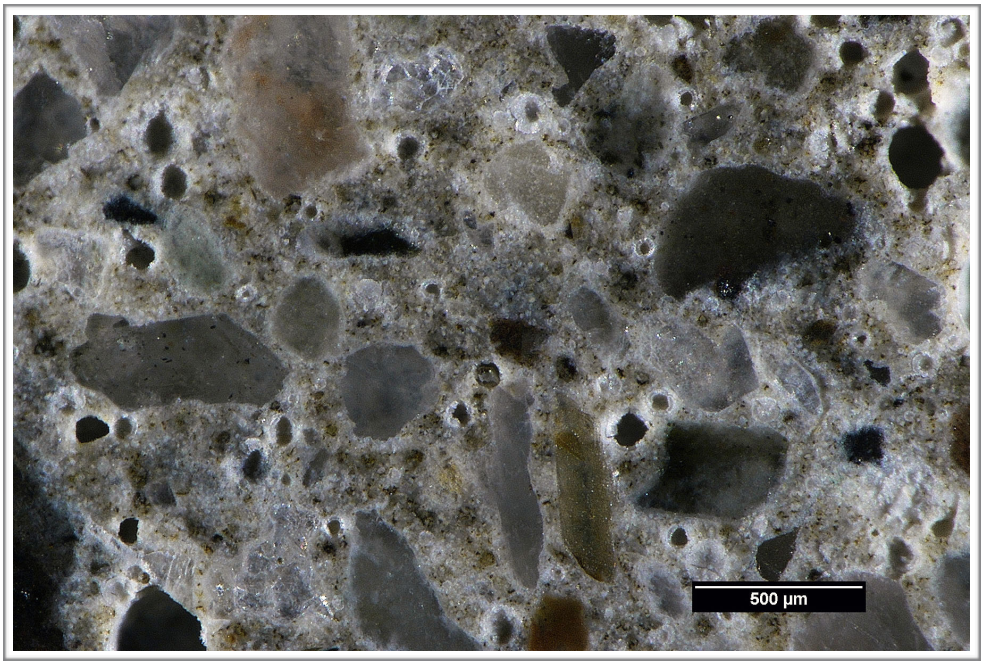

Figure A10. (a) Photograph of the polished surface showing overview of the paste at the top of the core.; scale in millimeters. (b) Reflected light photomicrograph of the polished surface showing detail of the paste in the middle of the core.

(a)

(b)

Figure A11. Photographs showing (a) overview and (b) detail of the fresh fracture; scale in millimeters in both images. The yellow arrows in (b) indicate ASR gel on the fracture surface.

(a)

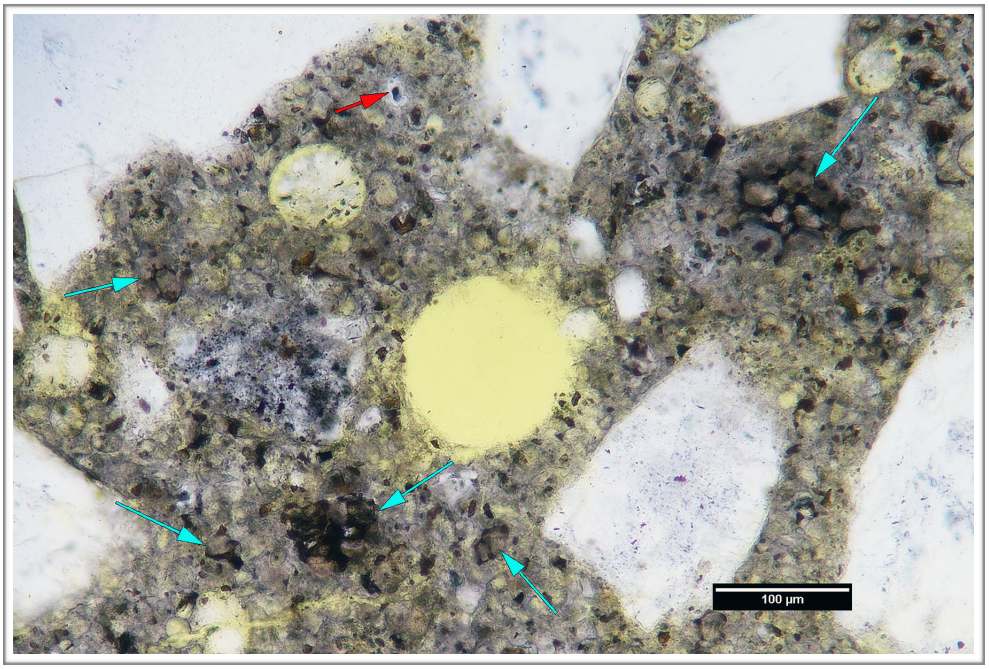

(b)

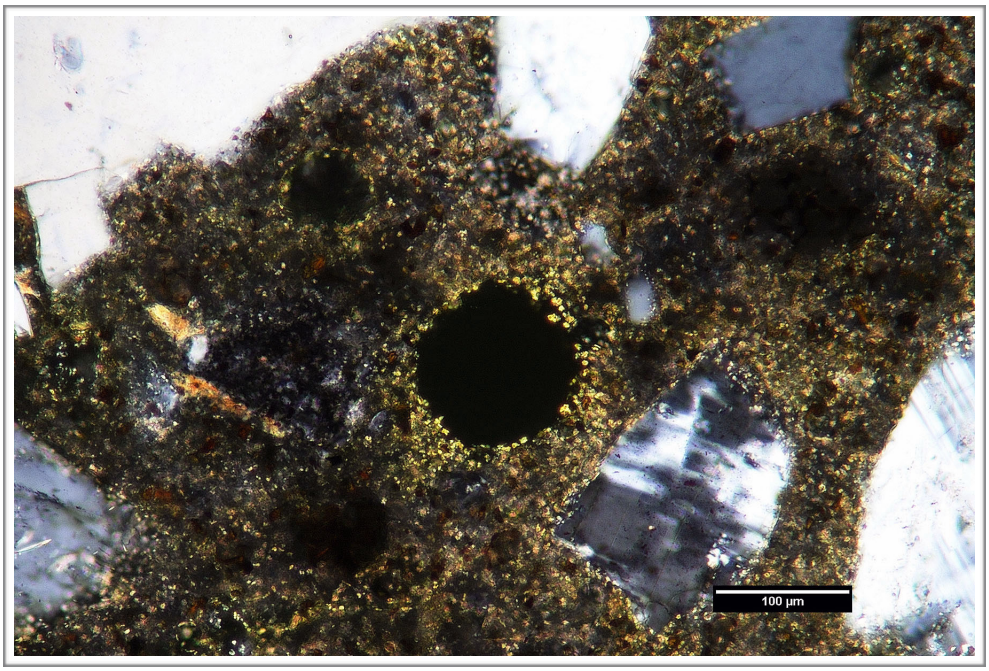

Figure A12. Transmitted light photomicrographs of thin section showing detail of paste in (a) plane-polarized and (b) cross-polarized light. In (a) the red and blue arrows indicate alite and belite, respectively.

(c)

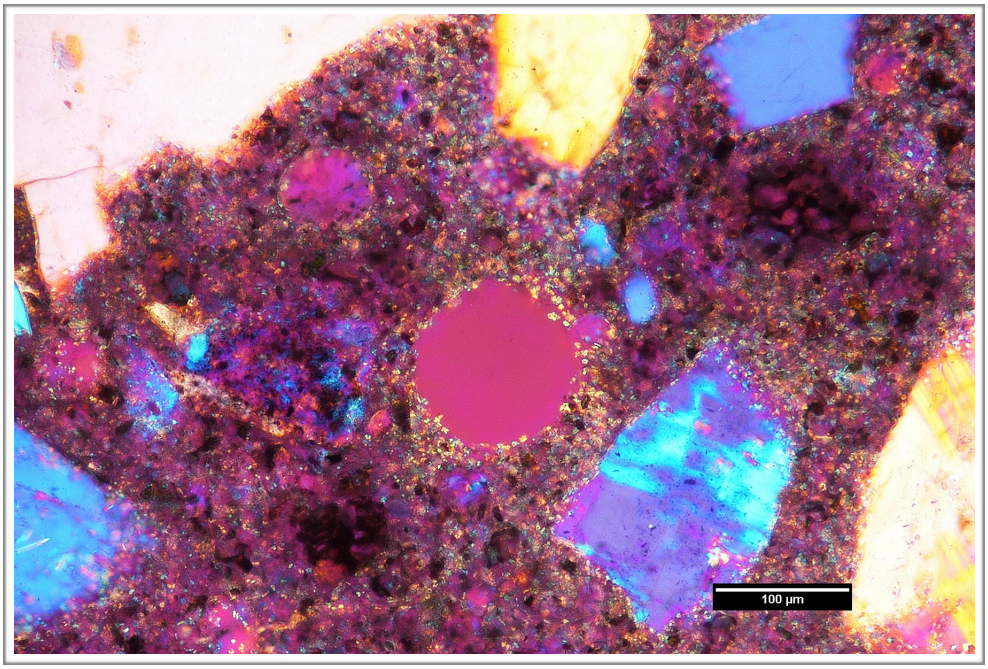

(d)

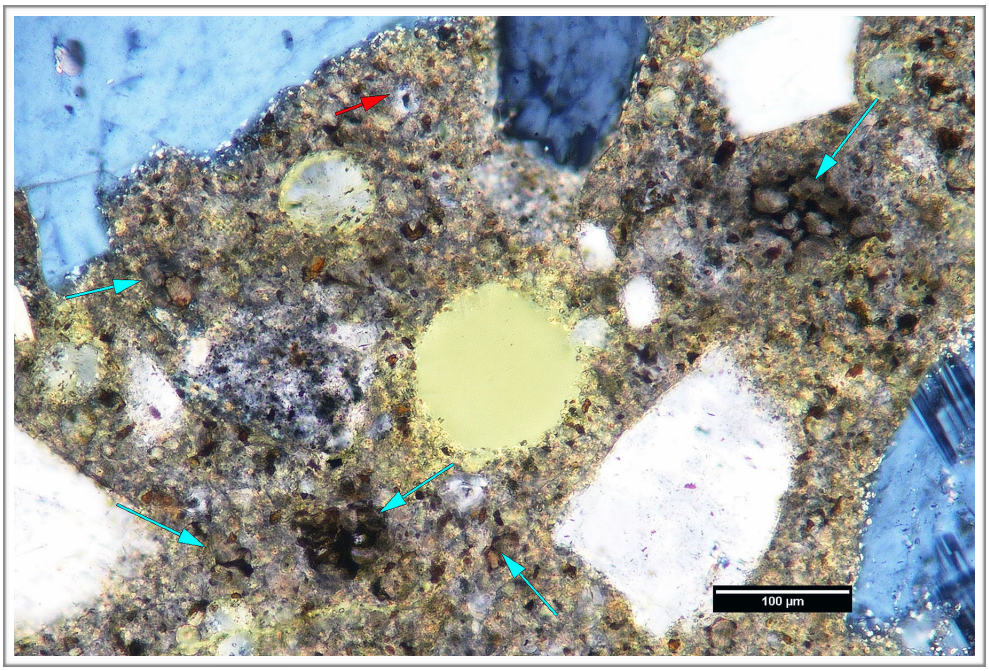

Figure A12 (cont'd). Transmitted light photomicrographs of thin section showing detail of paste in (c) cross-polarized light with the gypsum plate inserted and (d) cross-polarized light with the quarter wavelength plate inserted. In (d) the red and blue arrows indicate alite and belite, respectively.

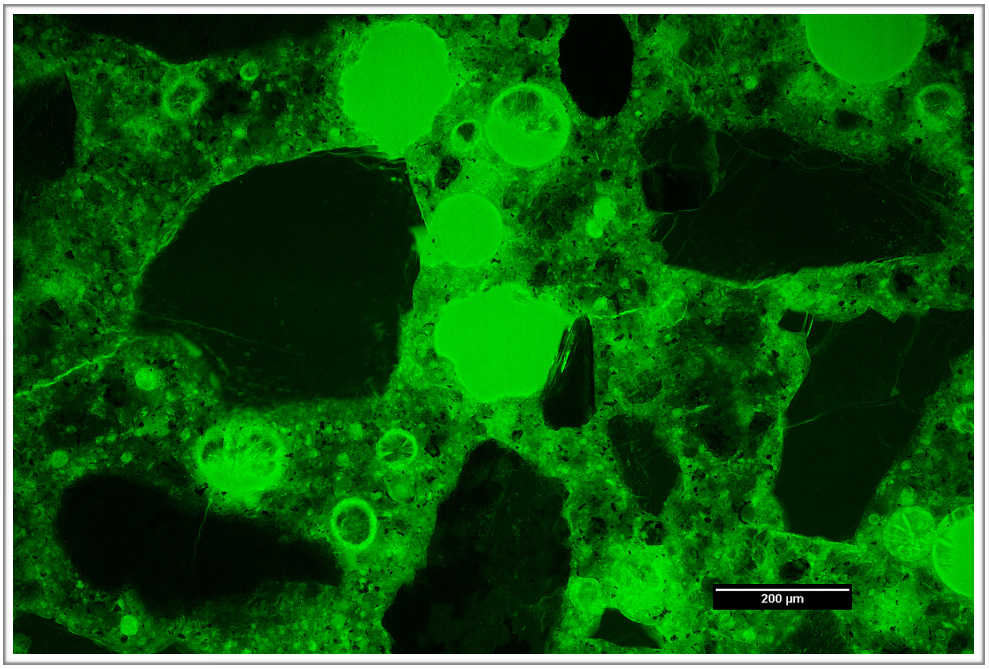

(a)

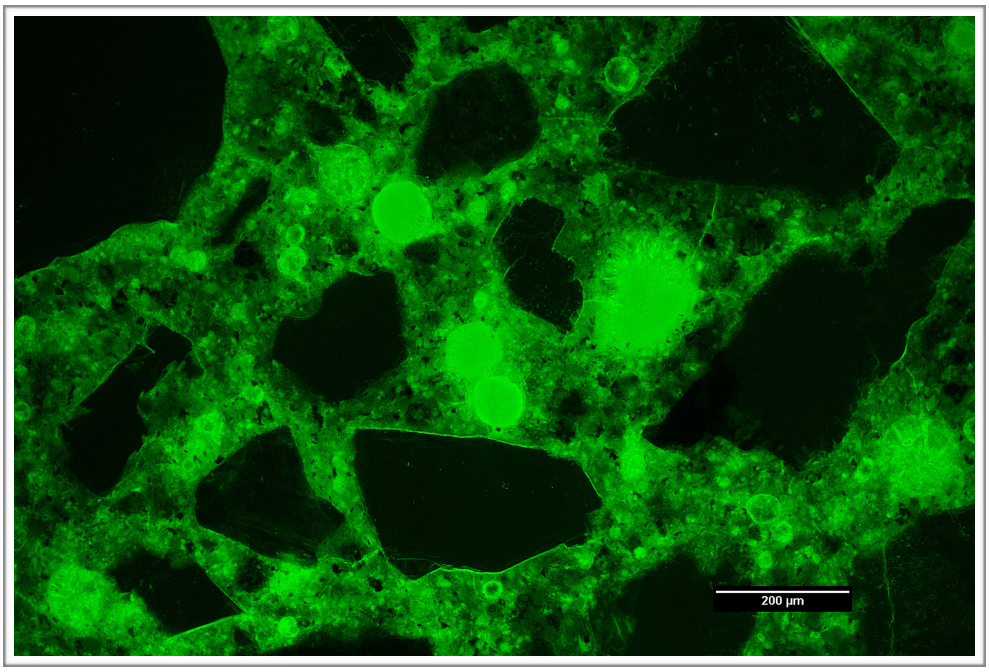

(b)

Figure A13. Transmitted fluorescent light photomicrographs of thin section showing detail of the capillary porosity of the paste. The black areas correspond to aggregate that has very low porosity and the bright green circles are air voids filled with epoxy. The variations in green between these end members reflect variations in the capillary porosity or micro-density of the paste. Note ettringite in voids.

(a)

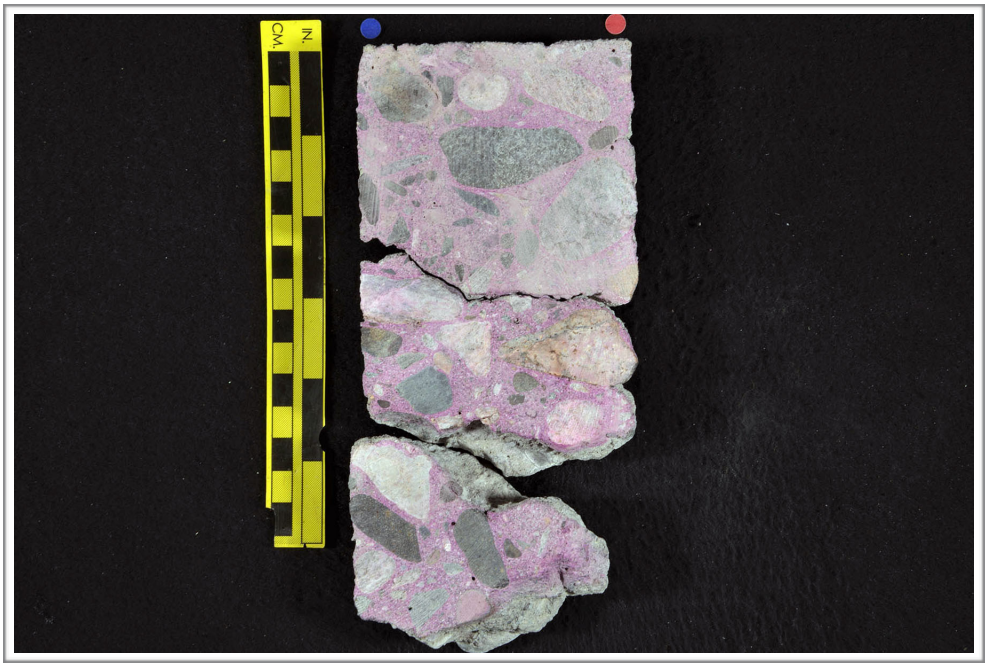

(b)

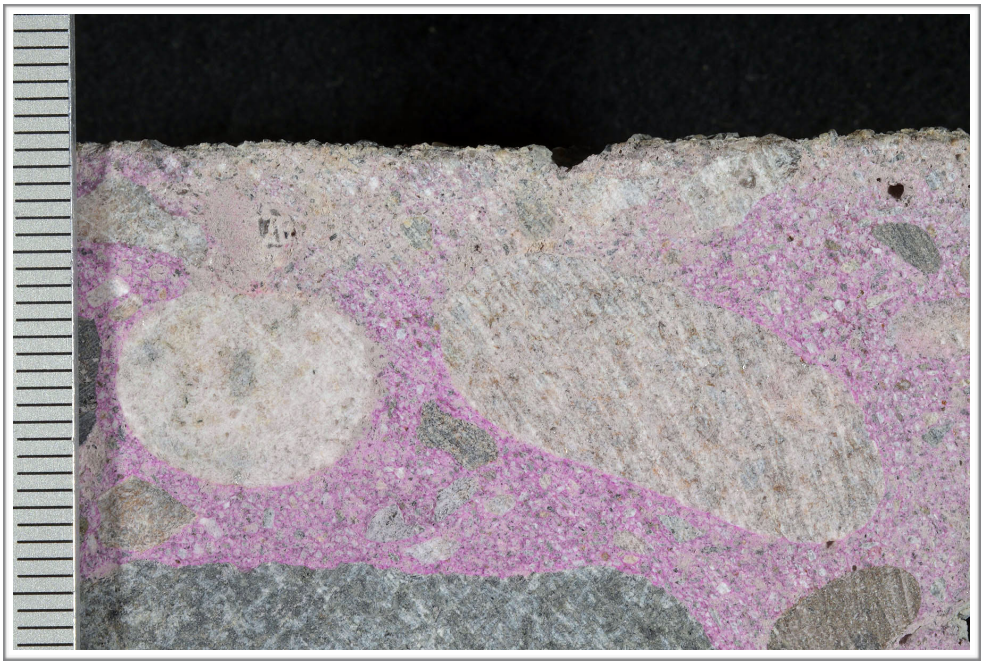

Figure A14. Photographs showing (a) overview of phenolphthalein-stained surface and (b) detail of surface near the top of the core. The yellow scale in (a) is ~ 150 mm (6 in.) long; the small and large divisions are in centimeters and inches, respectively. The scale in (b) is in millimeters.

1. Received Condition	
Orientation & Dimensions	Vertical core extracted from a bridge deck measures ~ 95 mm (3 ¾ in.) in diameter and is 165 – 195 mm (6 ½ – 7 ⅝ in.) long (**Figure B1, Figure B2**).
Surfaces	The top surface is worn and show fine aggregate particle (**Figure B3**) and the bottom surface is a fracture such that the core represents a partial thickness of the bridge deck.
General Condition	The concrete is hard and compact and rings lightly when sounded with a hammer. A sub-horizontal crack 60 – 90 mm (2 ⅜ – 3 ½ in.) below the top surface cuts the core into two pieces. Because the crack is open the original width cannot be measured. White deposits of ASR gel were observed lining voids and coarse aggregate particles on the bottom surface (**Figure B4**).

2. Embedded Objects	
General	None observed.

3. Cracking	
Macroscopic	A linear crack measuring ~ 90 mm (3 ½ in.) long and up to 750 µm (30 mil) wide strike across the top of the core (**Figure B5**). It cuts sub-vertically to 20 – 25 mm (¾ – 1 in.) from the top of the core, passing mainly around coarse aggregate particles. ASR gel fills the crack at the bottom. As described above, a sub-horizontal crack cuts the core in two 60 – 90 mm (2 ⅜ – 3 ½ in.) from the top surface. Two additional sub-horizontal cracks were observed at 60 – 90 mm (2 ⅜ – 3 ½ in.) from the top of the core. They sub-vertically strike across the core. They measure 50 mm (2 in.) long and up to 1 mm (40 mil) wide. The cracks occasionally cut through coarse aggregate particles and are filled with ASR gel. Additional relatively fine sub-vertical and sub-horizontal cracks were observed throughout the entire depth of the core. The cracks and microcracks are interconnected and form complex networks of cracking. They measure up to 50 mm (2 in.) long and up to 200 µm (8 mil) wide. They commonly cut throughout and radiate from aggregate particles and are filled with ASR gel.
Microscopic	Numerous microcracks were observed throughout the entire core (**Figure B6**). The microcracks are mainly in orientation and form an interconnected network. The microcracks measure up to 40 mm (1 ⅜ in.) long and up to 100 µm (4 mil) wide. They occasionally to commonly cut through aggregate particles and are partially filled with ASR gel.

4. Voids	
Void System	Concrete is air-entrained and contains ~ 6% total air as estimated from visual and microscopical observations (not measured in accordance with ASTM C457; **Figure B7**). Most of the air voids are smaller than 200 µm (8 mil) across. The concrete is well consolidated.
Void Fillings	Ettringite was commonly observed lining voids throughout the entire core. ASR gel was occasionally observed lining and filling voids throughout the entire core.

5. Coarse Aggregate

Physical Properties	The coarse aggregate is a crushed gravel that has a 19 mm (¾ in.) nominal top size (**Figure B8**). The rocks are hard and competent. The particles are sub-equant to slightly elongated with aspect ratios of 2:1. The particles have sub-angular to sub-rounded edges.
Rock Types	The aggregate is siliceous in composition and consist primarily of rhyolite with abundant phenocrysts of plagioclase and amphibole, granitic rocks, quartzite and chert. Minor amounts of andesite with abundant phenocrysts of amphibole and basalt were also observed. Abundant chlorite from hydrothermal alteration is present in rhyolite and granitic rocks. Rhyolite, granitic rocks, quartzite, chert and andesite are potentially susceptible to alkali-silica reaction (ASR).
Other Features	No deleterious coatings or incrustations observed. Low w/c mortar coatings were occasionally observed. Reaction rims were commonly observed. Internal cracking and microcracking were occasionally to commonly observed. Coarse aggregate particles occasionally show de-bounding. Deposits of ASR gel were commonly observed in internal cavities, microcracks radiating from it, de-bounding sockets and nearby voids.

6. Fine Aggregate

Physical Properties	The fine aggregate is a natural sand that consists of rocks that are hard and competent (**Figure B9**). The particles are mostly sub-equant to slightly elongated in shape with sub-rounded to sub-angular edges. The grading and distribution are relatively even.
Rock Types	The sand consists of siliceous rocks similar to that observed in coarse aggregate. The fines also contain fragments of quartz and chlorite. Rhyolite, granitic rocks, quartzite, chert and andesite are potentially susceptible to alkali-silica reaction (ASR).
Other Features	No deleterious coatings or incrustations observed. Internal microcracking and reaction rims were occasionally observed. Deposits of ASR were occasionally observed lining the microcracks and voids associated with fine aggregate particles.

7. Paste Observations

Polished Surface	Paste is light grey (2.5Y/7/1) and slightly mottled, has a smooth texture and a sub-vitreous luster (**Figure B10**). The paste is moderately hard (Mohs ~ 3.0). Fly ash was observed.
Fresh Fracture	Fracture surface is light gray, has a granular texture and a sub-vitreous luster (**Figure B11**). The fracture dominantly cuts through ~ 50% of coarse aggregate particles. ASR gel was observed on the fracture surface.
Thin Section	The paste contains hydrated portland cement with fly ash; no slag cement or other SCM were observed. The hydration of the paste is normal with 4-8% RRCG that consist primarily of belite grains with interstitial aluminoferrite; alite was rarely observed and is very fine-grained with hydration rims (**Figure B12**). CH is fine grained and evenly distributed and makes up less 3-6% of the paste.
Estimated w/cm	The capillary porosity of the paste is moderate and slightly heterogeneous (**Figure B13**). The estimated w/cm is not provided due to the elevated moisture level and secondary deposits.

** Abbreviations as follows: DSL = densified surface layer; RRCG = relict and residual cement grains; SCM = supplemental cementitious materials; CH = calcium hydroxide; ITZ = interfacial transition zone. Modal abundances are based on visual estimations.*

8. SECONDARY DEPOSITS	
PHENOLPHTHALEIN	Entire surface stains purple except for light purple staining in top ~ 2 mm (80 mil) of the core (**Figure B14**).
SECONDARY DEPOSITS	Carbonation was observed in top ~ 2 mm (80 mil) of the core. Deposits of gel were occasionally to commonly observed in voids and cracking/ microcracking throughout the entire depth of the core. Deposits of ettringite were observed commonly in voids throughout the entire depth of the core. ASR Rating: **Severe ASR**.

FIGURES

(a)

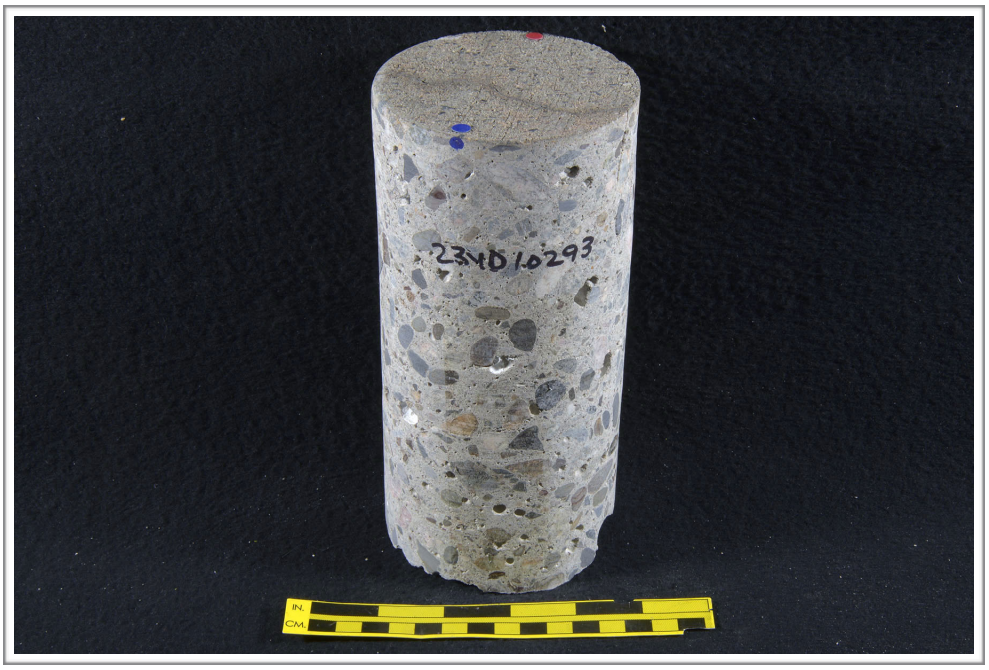

(b)

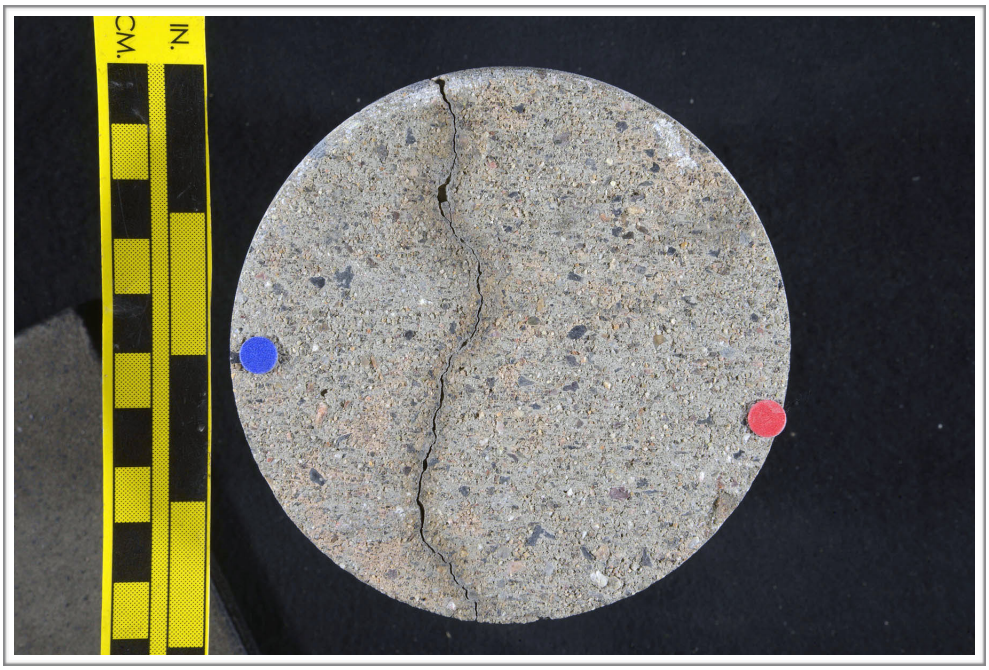

Figure B1. Photographs of the core in as-received condition showing (a) an oblique view of the top surface and side of the core with identification labels and (b) the top surface of the core. The red and blue dots show the orientation of the saw cuts used to prepare the core. The yellow scale is ~ 150 mm (6 in.) long; the small and large divisions are in centimeters and inches, respectively.

(c)

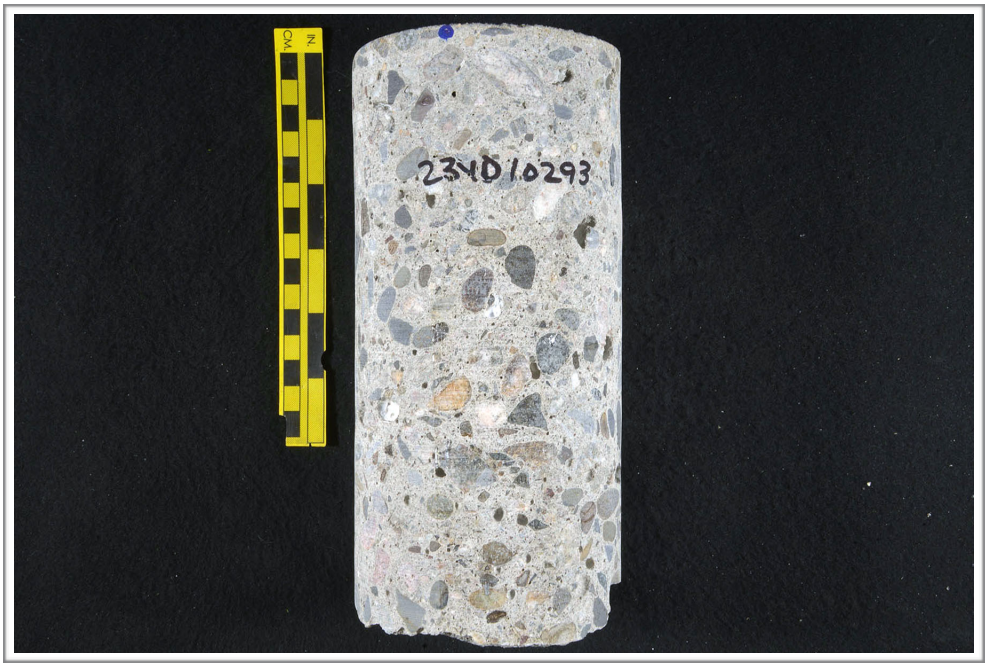

(d)

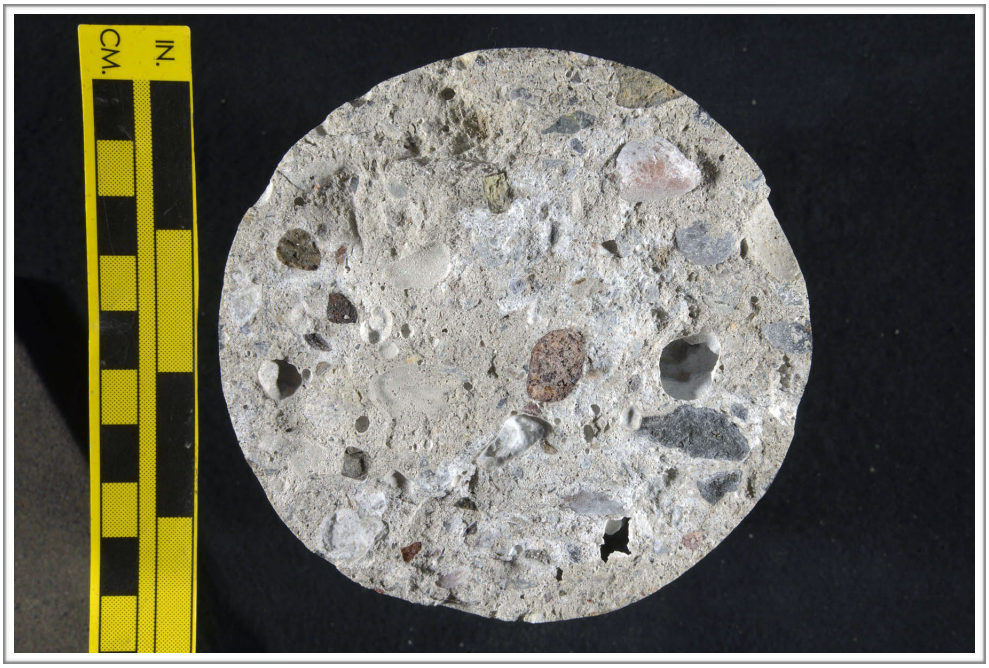

Figure B1 (cont'd). Photographs of the core in as-received condition showing (c) the side of the core and (d) the bottom surface of the core. The red and blue dots show the orientation of the saw cuts used to prepare the core. The yellow scale is ~ 150 mm (6 in.) long; the small and large divisions are in centimeters and inches, respectively.

Figure B2. Photograph showing the polished surfaces of the core. The small and large divisions on the yellow scale are in centimeters and inches, respectively.

Figure B3. Photograph showing detail of the top surface; scale in millimeters.

Figure B4. Photograph showing detail of ASR gel (yellow arrows) on the bottom surface of the core; scale in millimeters.

(a)

(b)

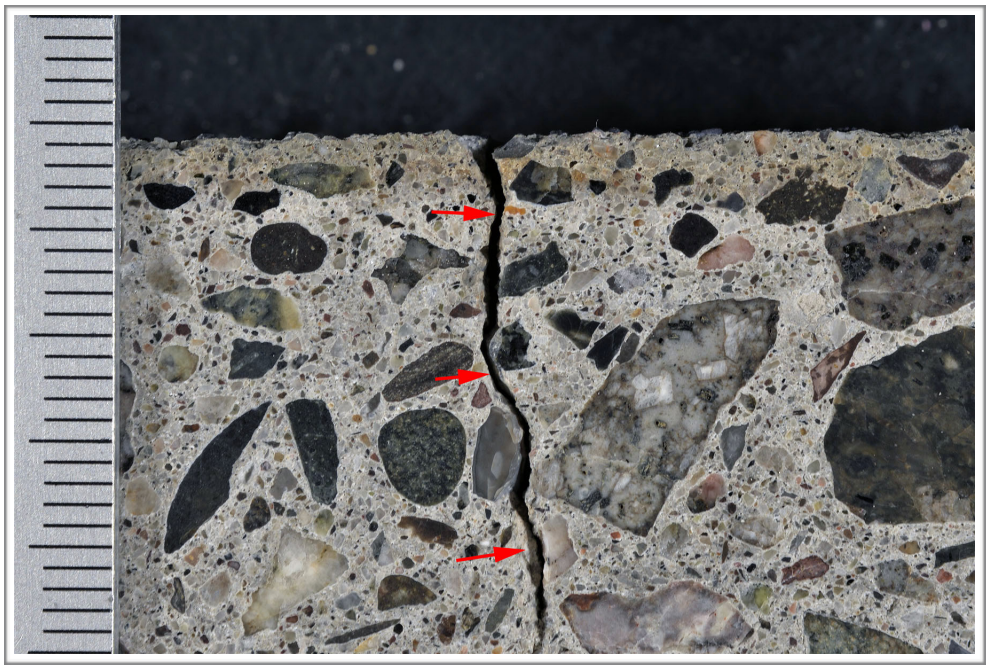

Figure B5. (a) Photograph of the top surface showing overview of the major crack (red arrows); scale in millimeters. (b) Photograph of the polished surface showing overview of the sub-vertical crack (red arrows) at the top of the core; scale in millimeters.

(c)

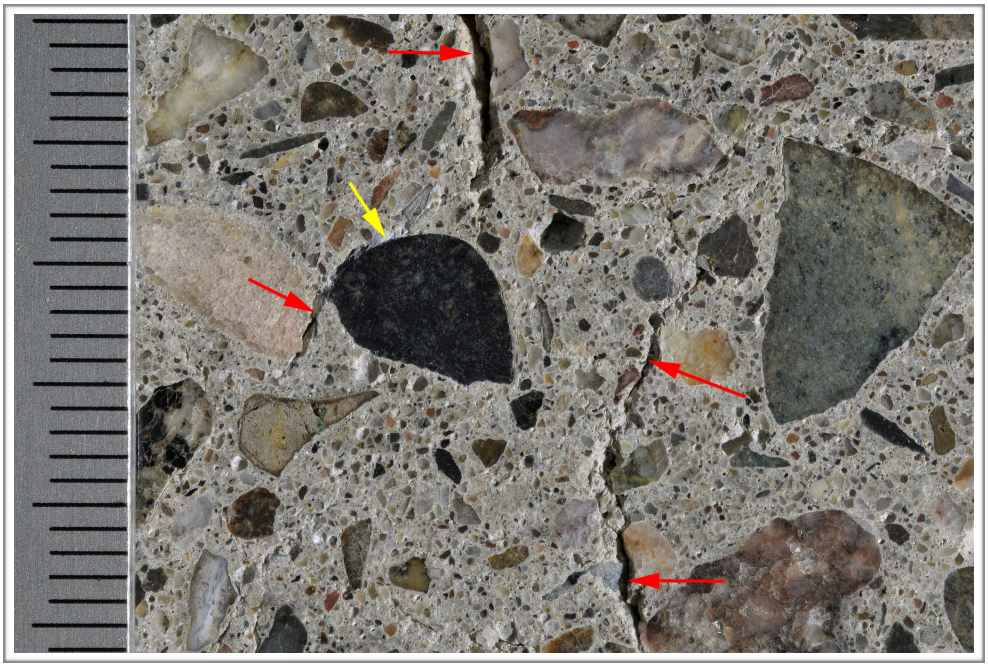

(d)

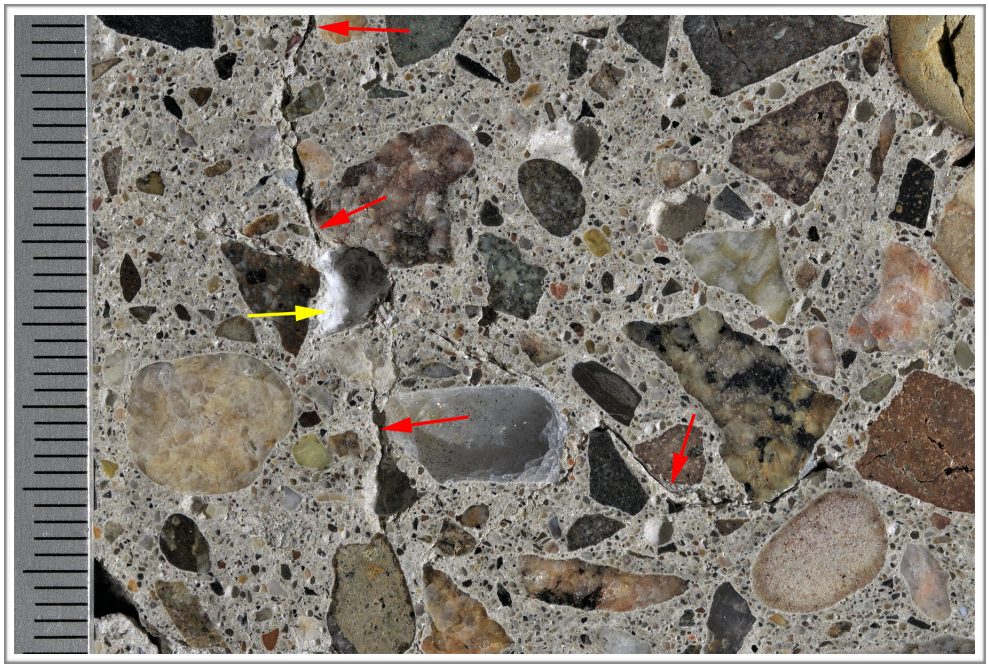

Figure B5 (Cont'd). Photographs of the polished surface showing overview of the sub-vertical and sub-horizontal cracks (red arrows); scale in millimeters. The yellow arrows indicate ASR gel.

(e)

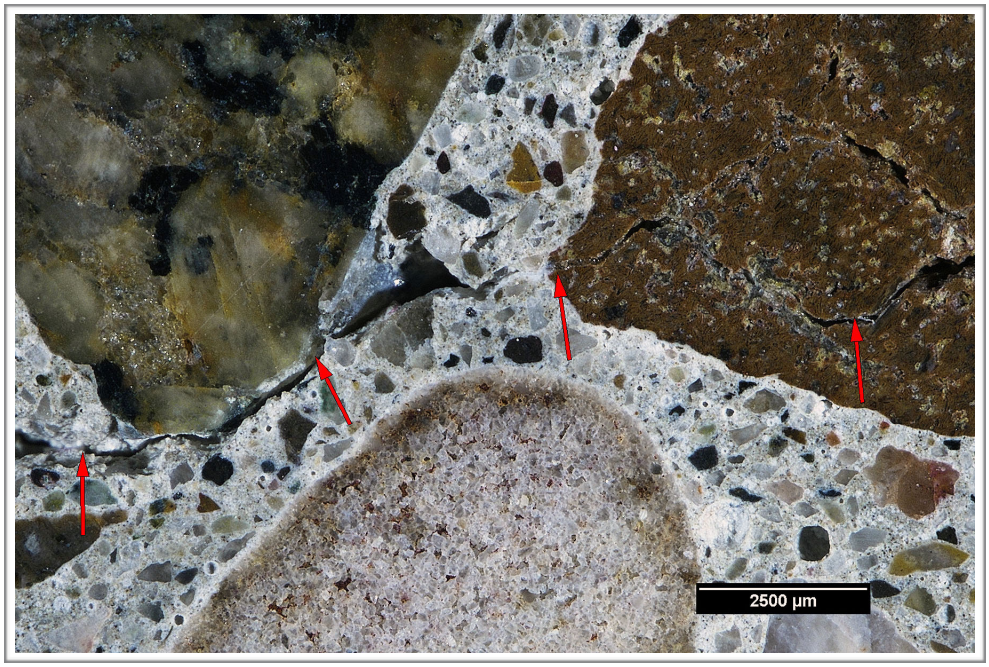

(f)

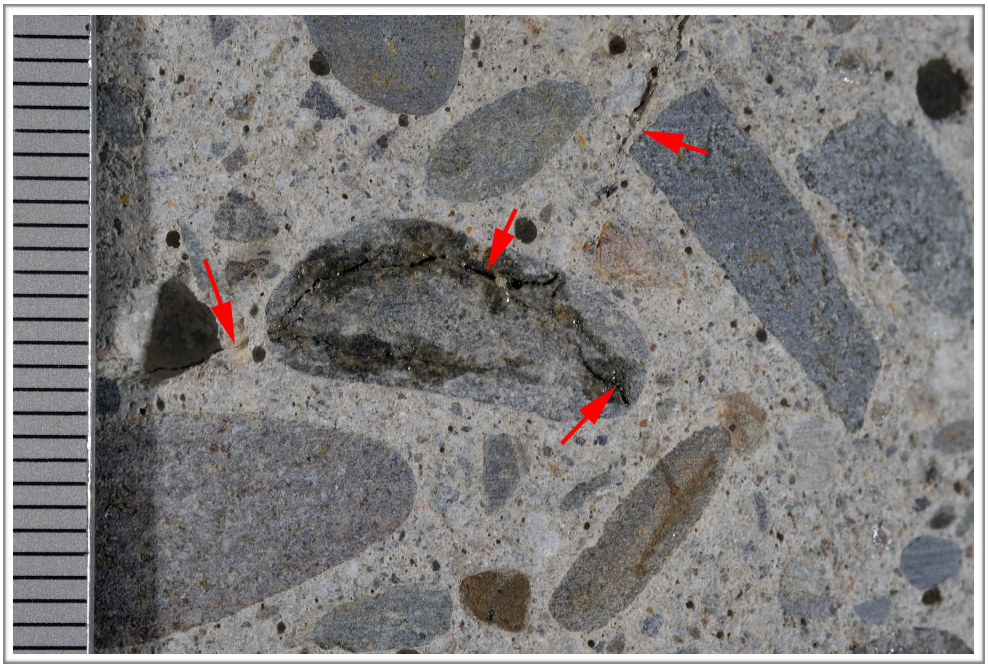

Figure B5 (Cont'd). (e) Reflected light photomicrograph of the polished surface showing overview of the sub-horizontal cracks (red arrows) cutting through a rhyolite particle. (f) Photograph of the side of the core showing overview of cracks (red arrows) radiating from an andesite particle. Note ASR gel in the crack in (e).

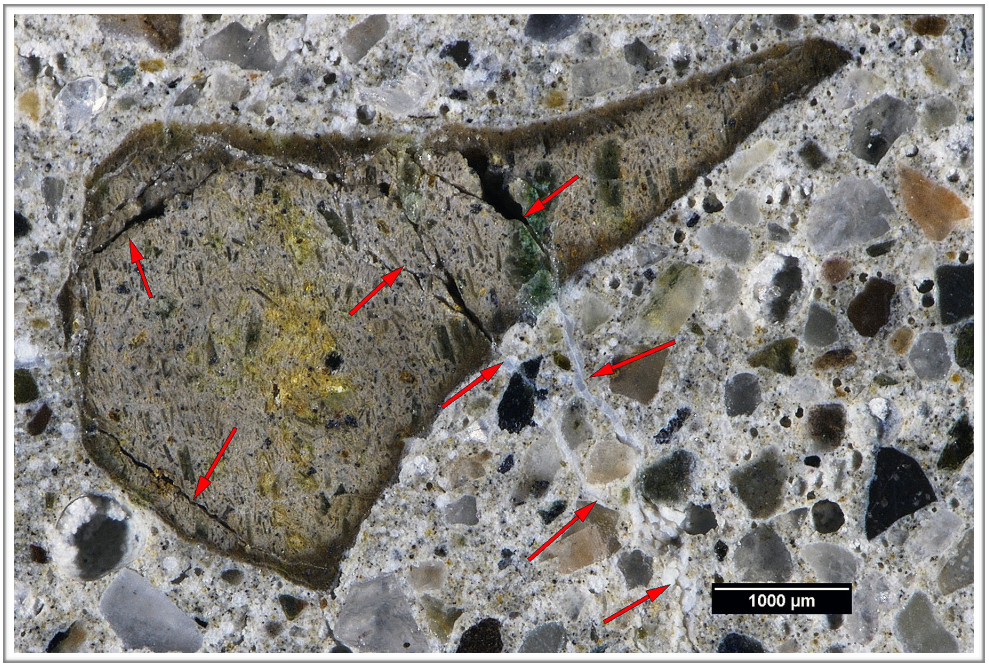

(a)

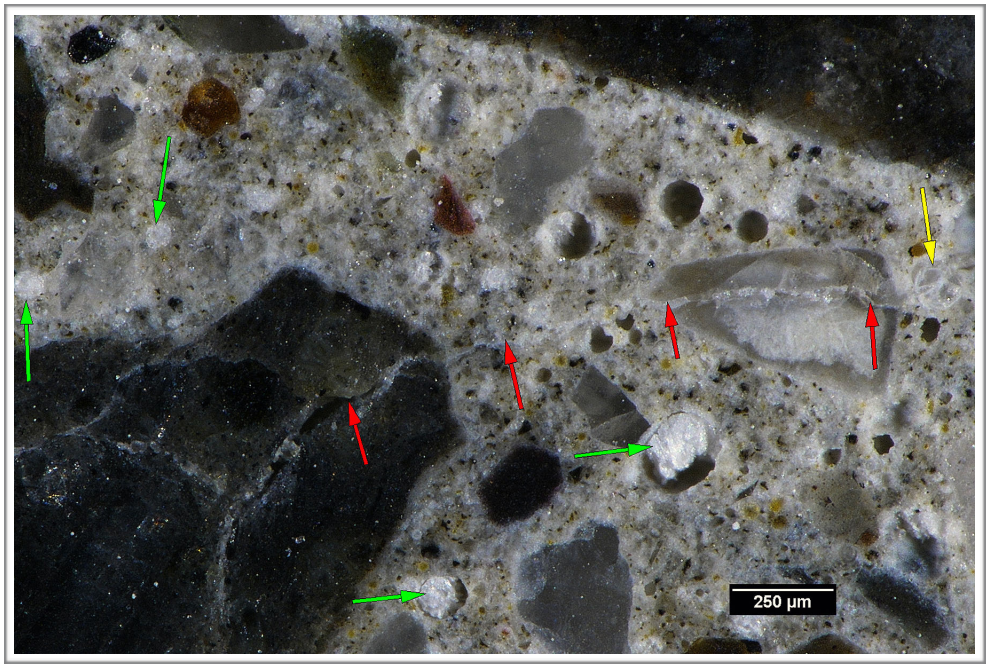

(b)

Figure B6. (a) Reflected light photomicrograph of the polished surface showing microcracks (red arrows) cutting through a rhyolite particle and filled with ASR gel. (b) Reflected light photomicrograph of the polished surface showing microcracks (red arrows) cutting through an andesite particle and filled with ASR gel. The yellow arrow in (b) indicates ASR gel lining a void. The green arrows in (b) indicate ettringite.

(c)

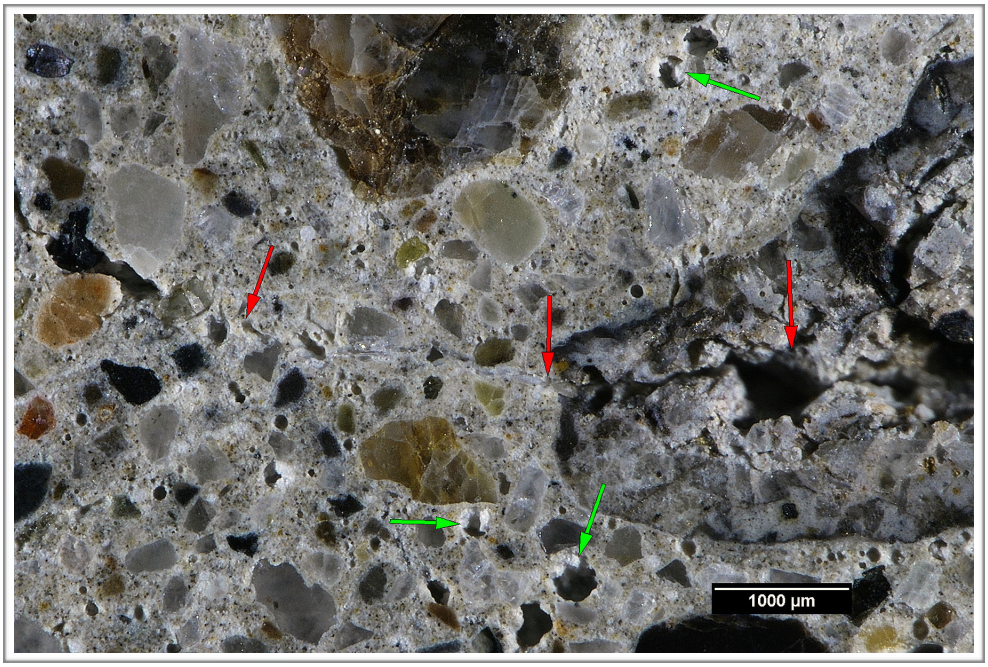

(d)

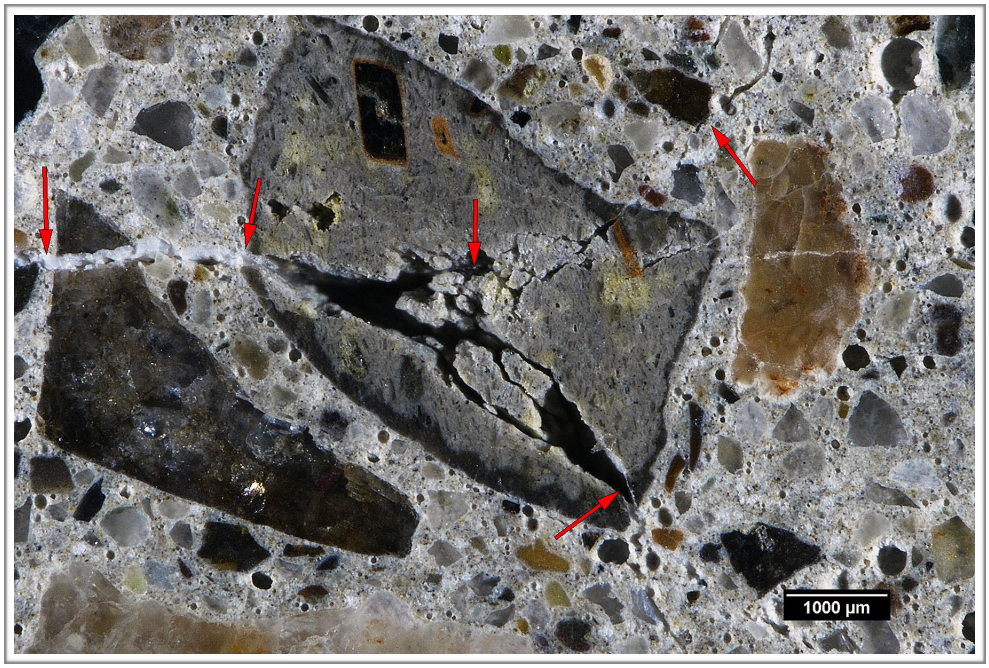

Figure B6 (Cont'd). (c) Reflected light photomicrograph of the polished surface showing microcracks (red arrows) cutting through a rhyolite particle. The green arrows in (c) indicate ettringite. (d) Reflected light photomicrograph of the polished surface showing microcracks (red arrows) radiating from a rhyolite particle and filled with ASR gel.

(a)

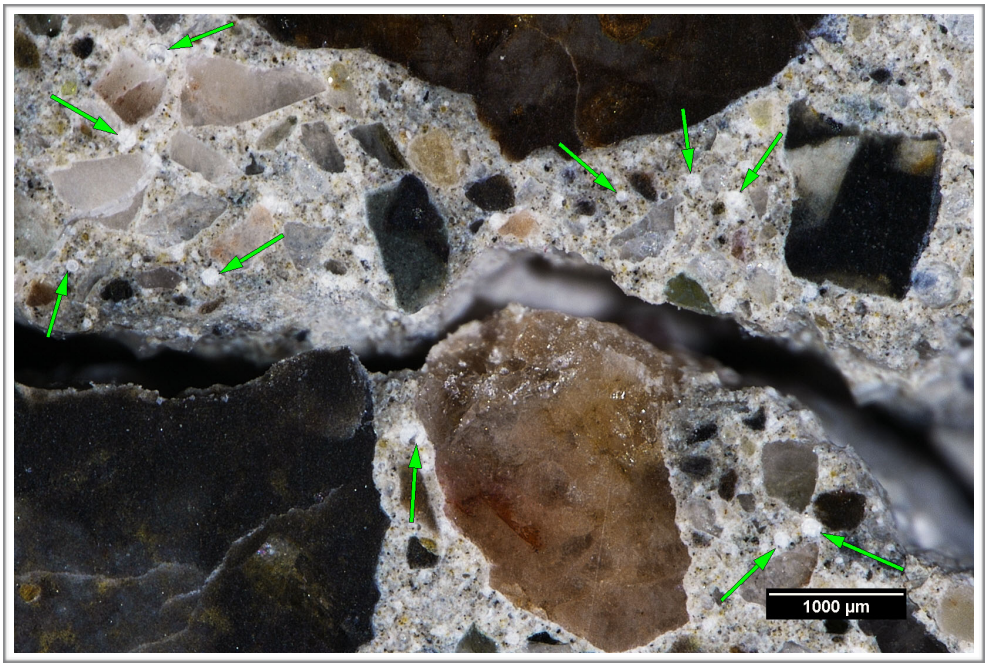

(b)

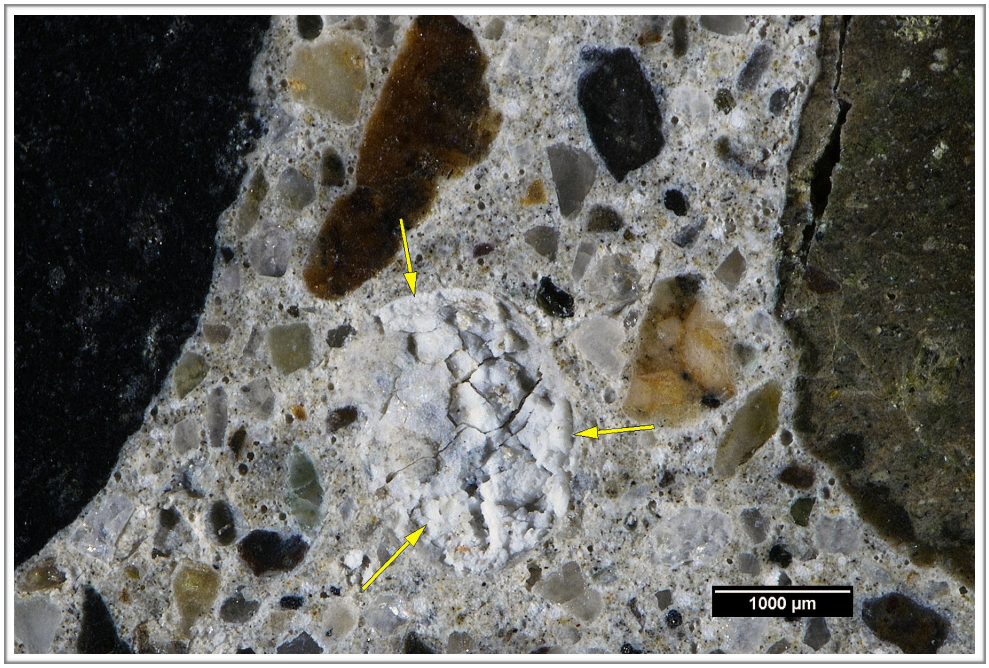

Figure B7. Oblique reflected light photomicrographs of the polished surface showing air voids filled with (a) ettringite (green arrows) and (b) ASR gel (yellow arrows) in the middle of the core.

(a)

(b)

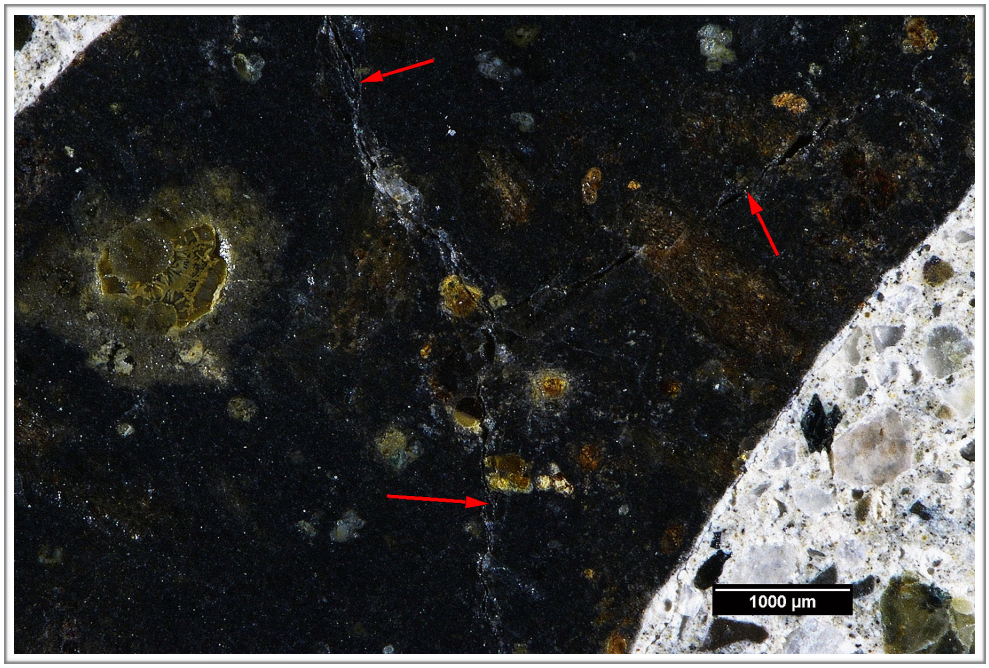

Figure B8. (a) Photograph of the polished surface showing overview of coarse aggregate; scale in millimeters. (b) Reflected light photomicrograph of the polished surface showing overview of a reacted andesite particle with internal microcracks (red arrows).

(a)

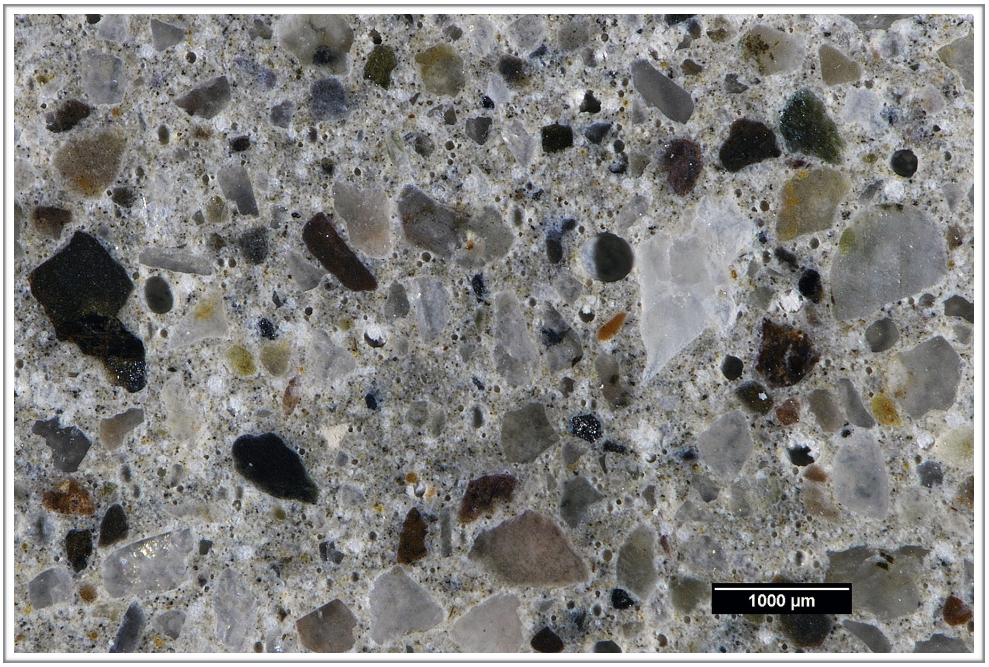

(b)

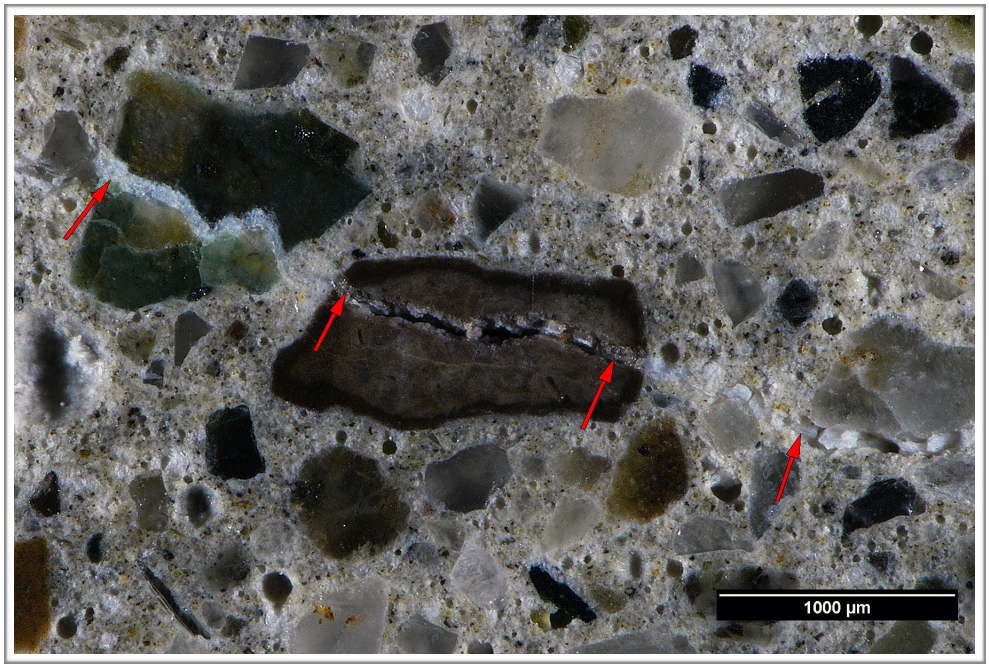

Figure B9. (a) Reflected light photomicrograph of the polished surface showing overview of the fine aggregate. (b) Reflected light photomicrograph of the polished surface showing overview of a rhyolite particle with microcracking (red arrows) with ASR gel cutting through it.

(a)

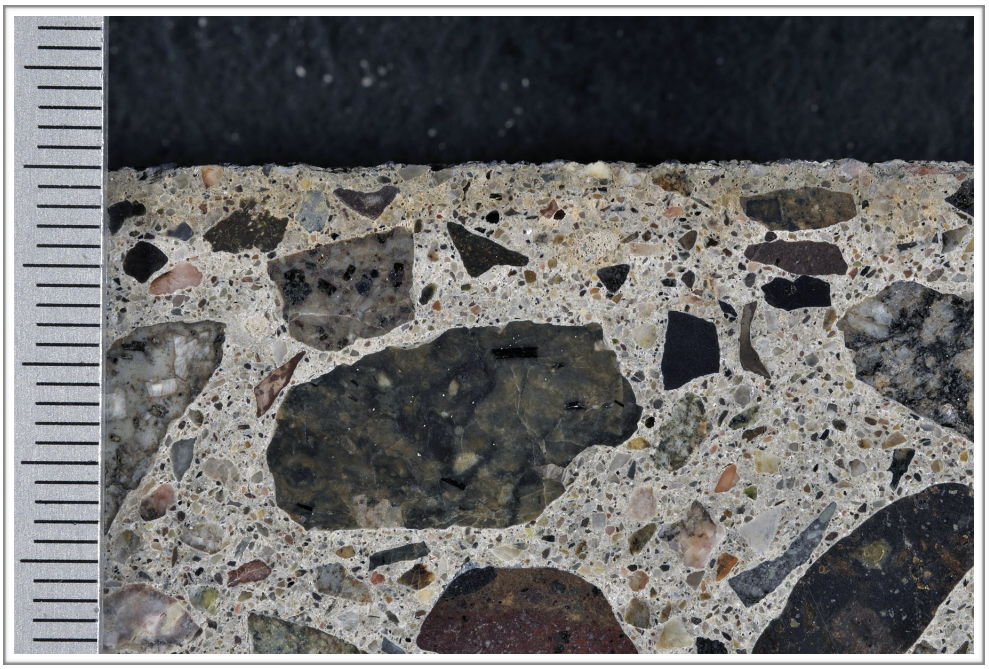

(b)

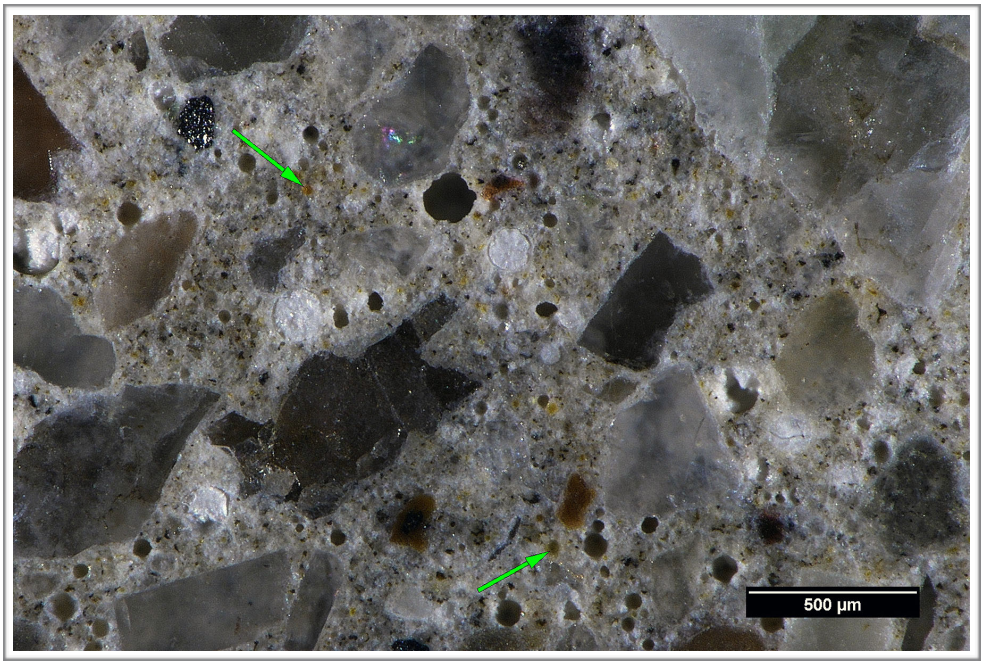

Figure B10. (a) Photograph of the polished surface showing overview of the paste at the top of the core.; scale in millimeters. (b) Reflected light photomicrograph of the polished surface showing detail of the paste in the middle of the core. The green arrows indicate fly ash.

(a)

(b)

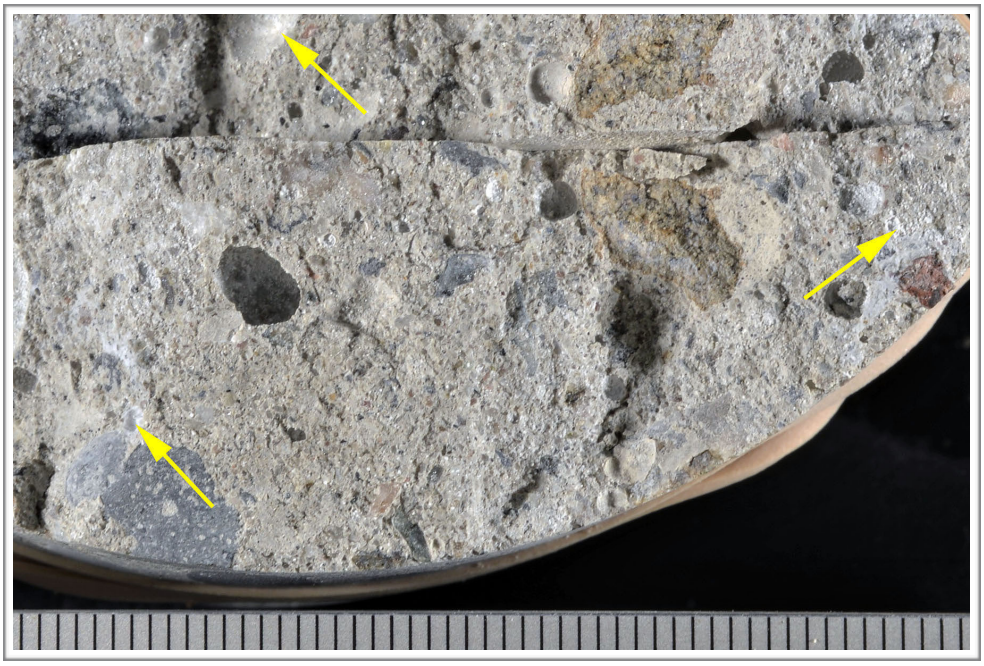

Figure B11. Photographs showing (a) overview and (b) detail of the fresh fracture; scale in millimeters in both images. The yellow arrows in (b) indicate ASR gel on the fracture surface.

(a)

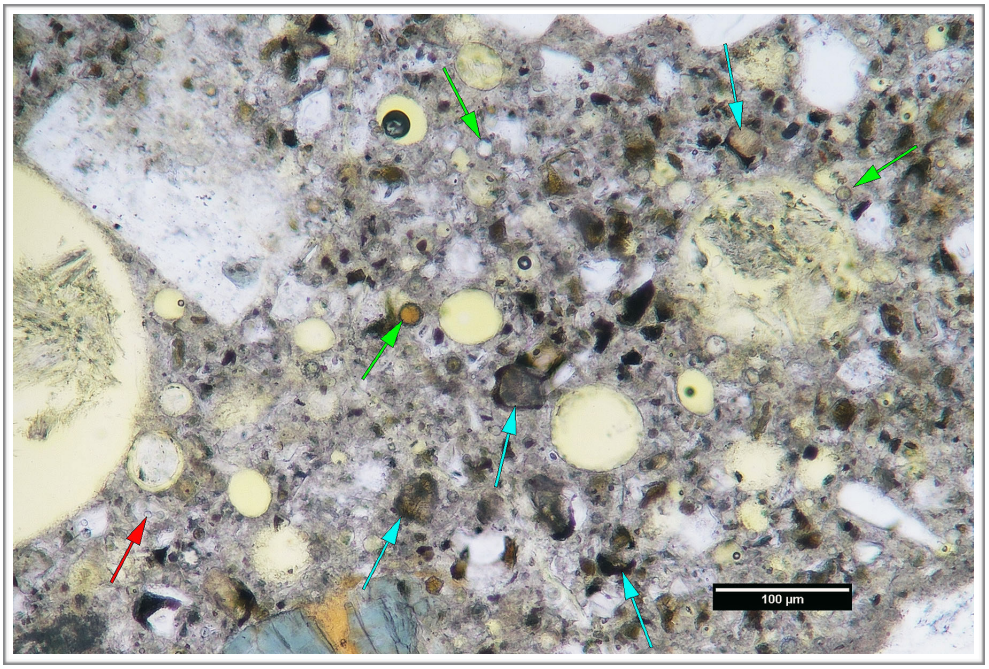

(b)

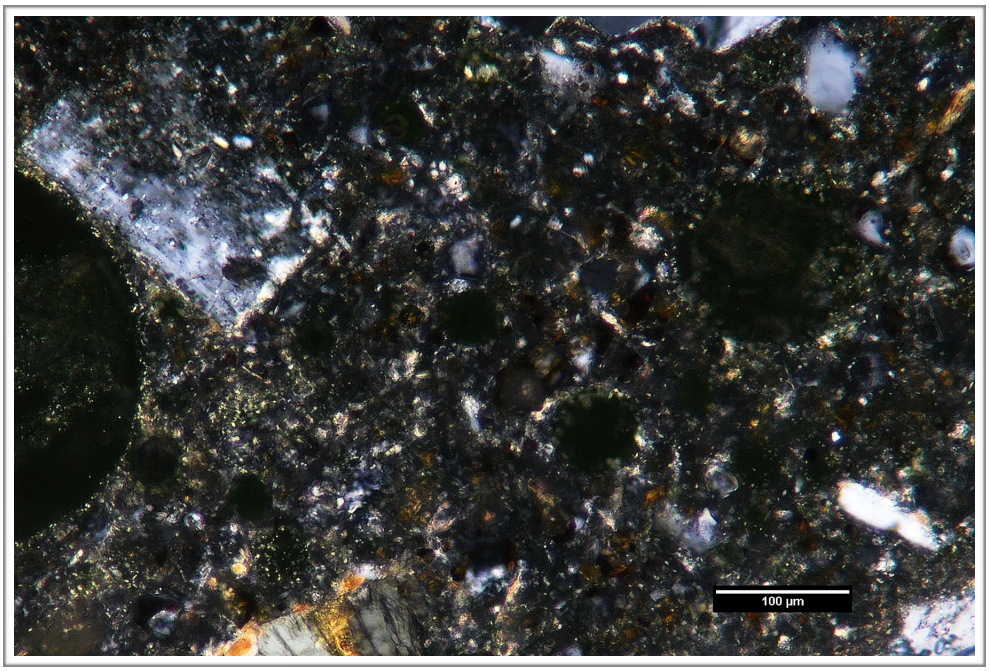

Figure B12. Transmitted light photomicrographs of thin section showing detail of paste in (a) plane-polarized and (b) cross-polarized light. In (a) the red, blue and green arrows indicate alite, belite and fly ash, respectively.

(c)

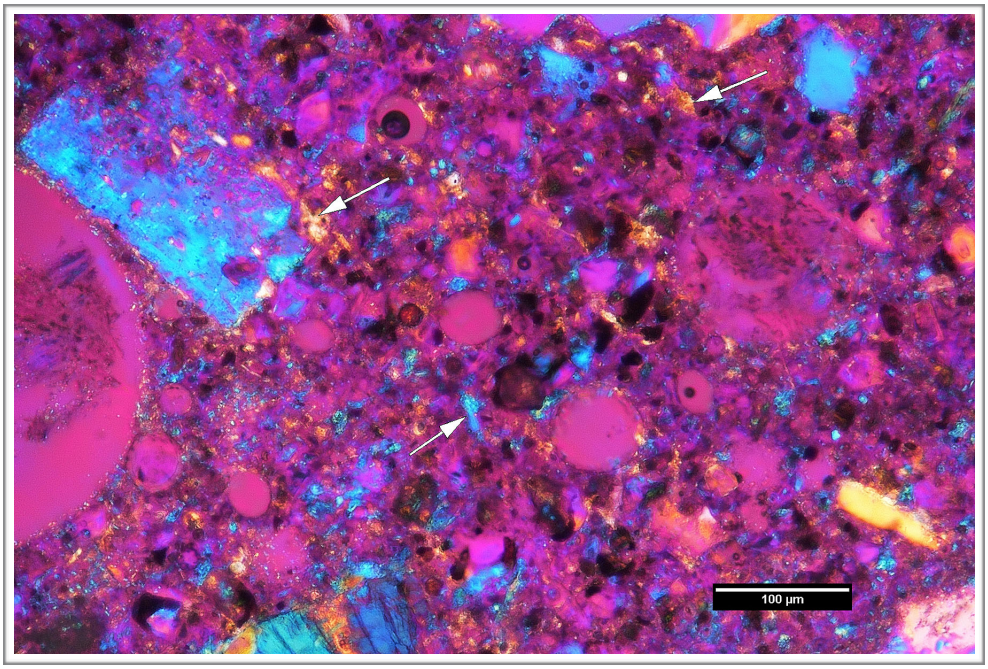

(d)

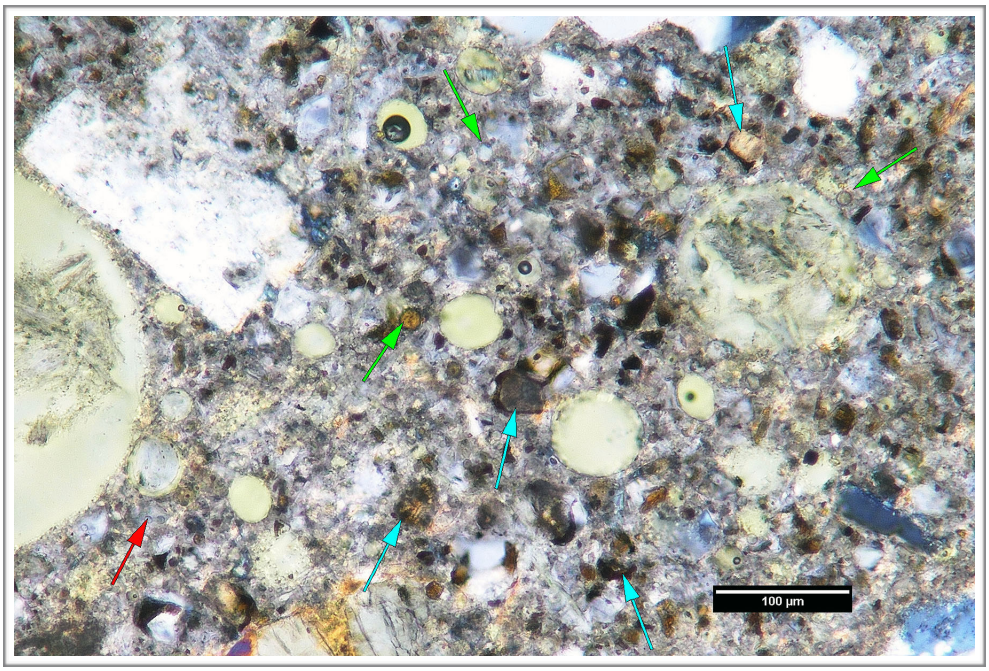

Figure B12 (cont'd). Transmitted light photomicrographs of thin section showing detail of paste in (c) cross-polarized light with the gypsum plate inserted and (d) cross-polarized light with the quarter wavelength plate inserted. The white arrows in (c) indicate calcium hydroxide. In (d) the red, blue and green arrows indicate alite, belite and fly ash, respectively.

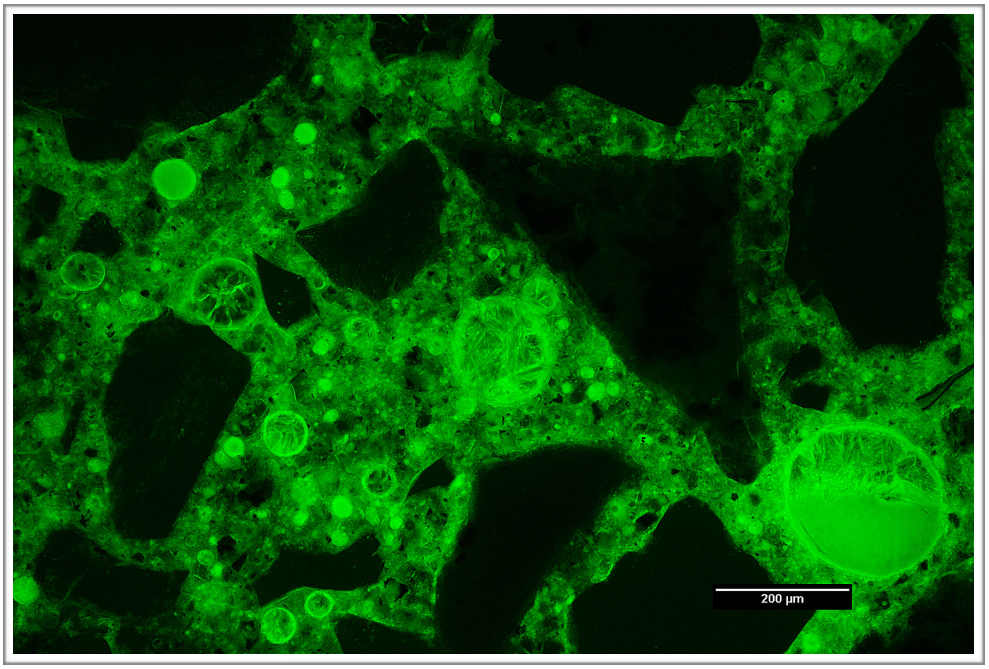

(a)

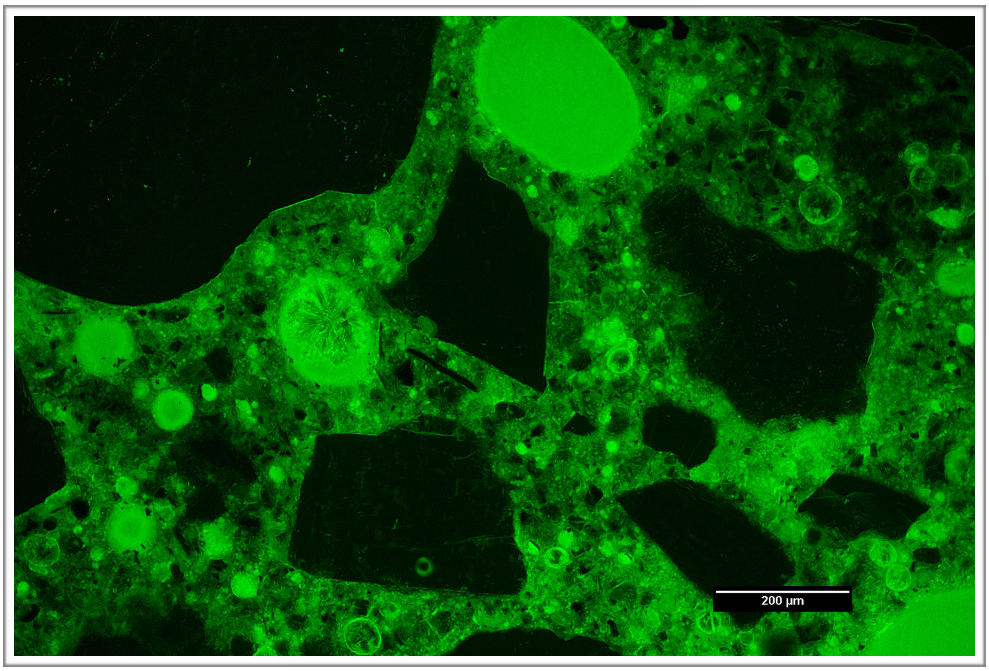

(b)

Figure B13. Transmitted fluorescent light photomicrographs of thin section showing detail of the capillary porosity of the paste. The black areas correspond to aggregate that has very low porosity and the bright green circles are air voids filled with epoxy. The variations in green between these end members reflect variations in the capillary porosity or micro-density of the paste. Note ettringite in voids.

(a)

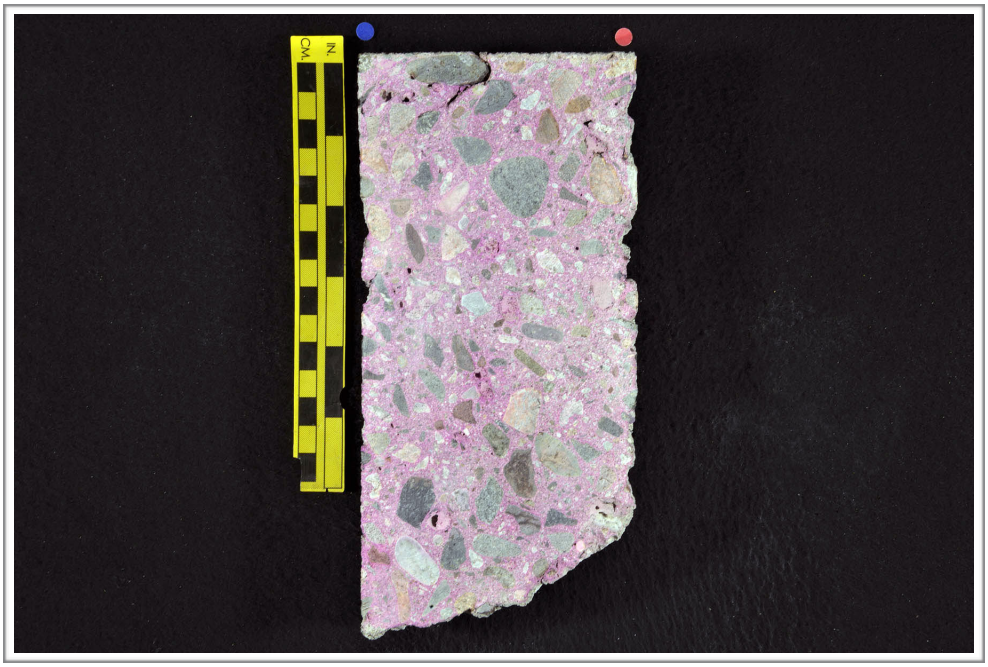

(b)

Figure B14. Photographs showing (a) overview of phenolphthalein-stained surface and (b) detail of surface near the top of the core. The yellow scale in (a) is ~ 150 mm (6 in.) long; the small and large divisions are in centimeters and inches, respectively. The scale in (b) is in millimeters.

PROCEDURES

ASTM C856--Petrographic Analysis The petrographic work was done following ASTM C856 [**1**] with sample preparation done at **DRP** in the following manner. After writing the unique **DRP** sample number on each sample near the received label, the samples were measured and inspected visually and with a hand lens. The orientation of the saw cuts used to prepare the samples was then indicated on each sample with blue and red dots. The samples were then photographed in their as-received condition.

A slab representing a longitudinal cross section of each sample was cut from the central portion of the core using a Diamond Pacific® TR-24, a 24-inch diameter oil-lubricated saw. This produced three (3) longitudinal sections for each core. These sections were rinsed in an aqueous solution with a detergent to remove the cutting oil and oven dried overnight in a Gilson® Bench Top laboratory oven at ~ 40°C (~ 105°F) to remove remaining traces of the oil. After drying, each piece was labelled with the appropriate **DRP** sample number. One piece was set aside for phenolphthalein staining and the other was set aside for thin section preparation.

The central slab was then lapped and polished on a Diamond Pacific® RL-18 Flat Lap machine. This machine employs an 18-inch diameter cast iron plate onto which Diamond Pacific® Magnetic Nova Lap discs with progressively finer grits are fixed. The Nova Lap discs consist of a $^{1}/_{16}$ in. backing of solid rubber containing magnetized iron particles that is coated with a proprietary Nova resin-bond formula embedded with industrial diamonds of specific grit. The slab preparation involved the use of progressively finer wheels to a 3000 grit (~4 μm) final polish following procedures outlined in ASTM C457 [**2**]. An aqueous lubricant is used in the lapping and polishing process. The polished slab from each sample was examined visually and with a Nikon® SMZ-25 stereomicroscope with 3-158 magnification capability following to the standard practice set forth in ASTM C856.

Phenolphthalein was applied to a freshly saw-cut surface from each sample to assess the extent of carbonation, along with thin section analysis. Phenolphthalein is an organic stain that colors materials with pH of greater than or equal to ~ 9.5 purple. Portland cement concrete generally has a pH of ~ 12.5. Carbonation lowers the pH of the paste below 9.5, so areas not stained by phenolphthalein are an indicator of carbonation. The depth of paste not stained by phenolphthalein was measured from each exposed surface.

1 *Standard Practice for Petrographic Examination of Hardened Concrete.* Annual Book of ASTM Standards, Vol. 4.02., ASTM C856-17.

2 *Standard Test Method for Microscopical Determination of Parameters of the Air-Void System in Hardened Concrete*, Annual Book of ASTM Standards, Vol. 4.02, ASTM C457-16.

Petrographic thin sections were prepared by cutting billets from the remaining longitudinal section. Outlines marking the area of the billets were drawn with a marker on the saw-cut surface after visual and microscopical examination of saw-cut and polished surfaces. The billets were labeled with the unique **DRP** number assigned to the sample and impregnated with epoxy. The impregnated billets were then fixed to glass slides with epoxy. After the epoxy cured, the slides were trimmed and ground on a Pelcon® Automatic Thin Section machine to a thickness of 20-25 µm (0.80-1 mil). The thin sections were examined with a Nikon® E-Pol 600 petrographic microscope equipped to provide a 20-1000x magnification range following the standard practice set forth in ASTM C856.

Capillary Porosity Measurement Measurement of the capillary porosity was done using image analysis methods and fluorescent microscopy of thin sections. Images were collected using constant lighting conditions. The images were binarized and analyzed using *Image J,* a freeware program available through the National Institute of Health (https://imagej.nih.gov/ij/download.html). The fluorescent signal recorded by each pixel in an image is tabulated to provide a distribution and a peak corresponding the paste is obtained. A peak corresponding to voids, which have a porosity of 100%, is used as a reference datum to provide a numerical measurement of the average porosity of the paste.